STUDY OF NANOCRYSTALLINE FORMATION OF MAGNETIC PROPERTIES IN $Fe_{72.5}Ag_2Nb_3Si_{13.5}B_9$ METALLIC RIBBON

M.Sc. Thesis

BY

MD. MAHMUDUZZAMAN TAWHID

DEPARTMENT OF PHYSICS
KHULNA UNIVERSITY OF ENGINEERING & TECHNOLOGY
KHULNA - 9203, BANGLADESH

MARCH - 2017

STUDY OF NANOCRYSTALLINE FORMATION OF MAGNETIC PROPERTIES IN $Fe_{72.5}Ag_2Nb_3Si_{13.5}B_9$ METALLIC RIBBON

M.Sc. Thesis

BY

MD. MAHMUDUZZAMAN TAWHID

ROLL NO: 1555552
SESSION: JULY-2015

A THESIS SUBMITTED TO THE DEPARTMENT OF PHYSICS, KHULNA UNIVERSITY OF ENGINEERING & TECHNOLOGY, KHULNA - 9203 IN PARTIAL FULFILMENT OF THE REQUIRMENT FOR THE DEGREE OF MASTER OF SCIENCE

DEPARTMENT OF PHYSICS
KHULNA UNIVERSITY OF ENGINEERING & TECHNOLOGY
KHULNA - 9203, BANGLADESH

MARCH- 2017

Dedicated

TO

MY PARENTS

DECLARATION

This is to certify that the thesis work entitled as **"Study of Nanocrystalline Formation of Magnetic properties in $Fe_{72.5}Ag_2Nb_3Si_{13.5}B_9$ Metallic Ribbon"** has been carried out in partial fulfillment of the requirement for M.Sc. degree in the Department of Physics, Khulna University of Engineering & Technology, Khulna-9203, Bangladesh. The above research work or any part of this work has not been submitted to anywhere for the award of any degree or diploma. No other person's work has been used without due acknowledgement.

1. **Supervisor** **Candidate**

....

Prof. Dr. Shibendra Shekher Sikder Md. Mahmuduzzaman Tawhid

Acknowledgements

I express all of my admiration and devotion to the almighty Allah, the most beneficial who has enabled me to perform this research work and to submit this thesis.

I wish to express my sincere appreciation and deepest sense of gratitude to my venerable teacher and supervisor Prof. Dr. Shibendra Shekher Sikder, Head, Department of Physics, Khulna University of Engineering & Technology (KUET), Khulna for suggesting the problem and for his affectionate guidance and inspiration during the course of this research work. He is always ready to provide a lucid explanation of the different concepts involved and critical reading of the script and subsequent corrections are much appreciated. Any mistakes that remain are of course mine. Without his constant supervision this thesis work could not performed.

I am deeply grateful to Aninda Nafis Ahmed Senior Engineer, Md. Rakibul Quadeer Engineer and Sajib Aninda Dhar Engineer, PP & PDC, Bangladesh Council of Scientific and Industrial Research (BCSIR), Dhanmondi, Dhaka-1205, Bangladesh, who helped me to understand annealing, XRD measurements and technical assistance in the laboratory and they were very much co-operative with me.

I am grateful to S. Manjura Haque, Head & Chief Scientific Officer, MSD, AECD, for providing kind opportunity to work in their laboratory of Material Science Division for experimental work.

I am deeply grateful to Dr. Nazrul Islam Khan, PSO, MSD, AECD for his help in XRD analysis of the materials. I am grateful to Eng. F M Kamal S.E., Dr. Md. Mahbubul Haque S. S. O. of MSD, AECD for providing me with technical assistance from time during my research work at the laboratory of AECD.

I am indebted to Prof. Dr. Md. Mahbub Alam, Prof. Dr. Abdullah Elias Akhtar and Prof. Dr. Jolly Sultana, Department of Physics, KUET for their extend in various ways the entire period of my study in this Department.

I am grateful to Mr. Md. Kamrul Hasan Reza, Associate Professor Department of Physics, KUET, Mr. Sujith Kumar Shil, Mr. Alamgir Hossain, Assistant Professor, Mr. Suman Halder , Mr. Suman Deb Nath , Lecture, Department of Physics, KUET for their tireless co-operation in my thesis work. I warm thanks to my well wishers and class fellows Robi and Shihab.

I am also thankful to Ms. Alhamra Parvin, E.O., Ms. Anjummanara Begum J. E. O., Mr. Anawar Hossain S. S. A. Ms. Nazmunnahar Begum (S. A.-II), Ms. Jarna

Begum (S. A.-II) of MSD, AECD, for their co-operation during the experiments and heartfelt help during the entire period of my research work at the laboratory of AECD. My thanks are due to the Director, MSD, AECD for his kind permission to use the laboratory of MSD, AECD.

A very special thanks to Mrs. Nandita Saha, spouse of Prof. Dr. S. S. Sikder for her heartfelt encouragement, cares and helps throughout the entire period of M. Phil. program.

I also wish to thanks the authority of Khulna University of Engineering & Technology (KUET), Khulna for providing me with the necessary permission and financial assistance for conducting this thesis work.

Md. Mahmuduzzaman Tawhid

ABSTRACT

This thesis focuses on the experimental investigation of the effect of grain size and phase constitution on the magnetic properties of $Fe_{72.5}Ag_2Nb_3Si_{13.5}B_9$ alloys in the amorphous and annealed states. The sample has been prepared by rapid solidification technique and their amorphous nature has been confirmed by X-ray diffraction (XRD). The crystallization behavior and the nanocrystal formation have been studied by Differential Thermal Analysis (DTA) and XRD. Magnetization measurements have been carried out using vibrating sample magnetometer (VSM). The ribbon sample has been annealed in a controlled way in the temperature range 550^{o}C to 750^{o}C for 2 hours. DTA runs for the sample show the existence of one exothermic peak for α-Fe(Si) phase. Thermal analysis experiment and from the obtained data activation energy of primary crystallization products α-Fe(Si) phase is 5.78 eV. The XRD experiments are in order to study the effect of structural parameters such as lattice parameter, crystallites size and silicon content of the nanocrystalline α-Fe(Si) grain. In the optimized annealing condition the grain size has been obtained in the range of 50 - 69nm. The peak shift indicates the change of the values of Si-content of nanograins and therefore, the change of the lattice parameter of nanograins. The saturation magnetization (M_s) has been observed 114emu/gm and in as prepared condition Curie temperature (T_c) has been found to be 305^{o}C. The critical composition for disappearance of ferromagnetism fall of curves M_s with the replacement Cu by Ag of FINEMET, where the nearest neighbor coupling to longer dominant and intermediate range occurs and the magnetization process of this amorphous ribbon sample are soft behavior of magnetic material.

CONTENTS

CHAPTER-III

EXPERIMENTAL DETAILS

CHAPTER-IV

RESULTS AND DISCUSSION

CHAPTER-V

CONCLUSIONS

List of Figures

List of Tables

List of Symbols

a_0	=	Lattice parameter
B	=	Magnetic induction
D_g	=	Grain size
DTA	=	Differential Thermal Analysis
DSC	=	Differential Scanning Calorimetry
d	=	Average diameter
FWHM	=	Full Width at Half Maximum
H	=	Magnetic field
H_c	=	Coercivity
H_a	=	Applied magnetic field
[hkl]	=	Miller Indices
k	=	Magnetic hardness parameter
K_B	=	Boatman's constant
K_{eff}	=	Effective magnetic anisotropy constant
L	=	Self inductance of the sample core
L_o	=	Inductance of the winding coil without sample
L_{ex}	=	Ferromagnetic exchange length
M	=	Magnetization
M_s	=	Saturation magnetization
nm	=	nano meter
NM	=	Nobel metal
RAM	=	Random anisotropy model
RDF(r)	=	Radial Distribution Function
S	=	Total spin angular momentum
T_{ij}	=	Exchange interaction between atoms at the position r_i and r_j.
TTT	=	Temperature, time & transformation
T_a	=	Annealing temperature
T_c	=	Curie temperature
T_g	=	Glass transition temperature
T_x	=	Crystallization temperature
T_m	=	Melting pointtemperature
T_{x_1}	=	Primary crystallization temperature
T_{x_2}	=	Secondary crystallization temperature

T_{p_1}	=	Primary crystallization peak temperature
T_{p_2}	=	Secondary crystallization peak temperature
VSM	=	Vibrating Sample Magnetometer
XRD	=	X-ray diffraction
μ	=	Permeability
λ	=	Wave length
θ	=	Scattering angle
t_o	=	Time constant
β	=	Heating rate
δ_w	=	Domain wall Width
σ	=	Effective stress
$\rho(r)$	=	Atomic density
$< K >$	=	Average anisotropy
T_c^{am}	=	Curie temperature of residual amorphous matrix
ΔH	=	Enthalpy of crystallization
ΔE	=	Activation Energy

INTRODUCTION

1.1 Introduction

Magnetism is one of the basic properties of materials. Magnetism appears in various forms, but one of the kinds that have practical value and therefore interests us is soft magnetic materials. The term 'soft' means temporary in the sense that ferromagnetism emerges only when a magnetic field is applied. Soft magnetic materials are basically required to have high initial or maximum permeabilities or susceptibilities and low losses; that is to say, the permeabilities should remain high over a consider range of frequencies. Soft magnetic materials face demanding requirement from new, high performance electronic and power distribution systems. The new system must operate in high temperature and high frequency regimes that are inaccessible to conventional crystalline and amorphous magnetic materials. The need for increased energy sufficiency requires reduced power loss from inductive components.

The enhancement of soft magnetic properties requires reduction of crystalline grain size to a much smaller length scale that can overcome the anisotropy effects and result in an improved soft magnetic behavior. This needs for a look into 'Nanoscience' which has made immense progress in previous respect within the last decades. Magnetic nanoparticles show a variety of unusual magnetic behavior when compared to that of the bulk materials due to the surface/interface effects including symmetry breaking, electronic environment/charge transfer and magnetic interactions. Nanocomposite/ nanocrystalline magnetic materials have been developed through appropriate heat treatment of the initial amorphous precursors of the Fe-Si-B and Co-Si-B based alloys for the ultra soft magnetic properties with extraordinary high permeability and Fe-Nb-B based alloys for the spring exchange hard magnets with high energy product. These technically important materials have enormous applications such as transformers, sensors for the soft magnetic materials and motor, actuators or generators for the hard nano composite magnetic materials.

Nowadays, the attempts to understand different properties of materials on a smaller and smaller length scale are making footsteps for development of research in many areas of material science. With the reduction of size into nanometer range, the materials exhibits interesting properties including physical, chemical, mechanical,

magnetic and electrical, comparting to conventional coarse-grained counterparts. This new field based on nanomaterials has been named as 'Nanotechnology' and emerged as a new branch of science and technology. It has been well established by the time through extensive research work that the addition of Cu and Nb, simultaneously with Fe-Si-B based amorphous alloys is the necessary condition for the extraordinary soft magnetic alloys called FINEMET having composition $Fe_{73.5}Nb_3Cu_1Si_{13.5}B_9$, , developed in 1988 by Yoshizawa, Oguma and Yamauchi at Hitachi Metals Ltd. [1.1]. The Cu additives play a key role in the formation of the nucleation centres and Nb by inhibital the grain growth [1.2]. This addition extends the temperature range between the primary crystallization of α-Fe(Si) phase and secondary crystallization Fe_2B phase for achieving superior magnetic properties [1.3]. It should be stressed again that good soft magnetic properties require not only a small grain size but at the same time the absence of boron compounds. Nanomaterials are generally materials that can have one dimension, two dimension or three dimension and can be specified within a size of 100 nanometer ($1nm=10^{-9}m$).

The separation between the primary crystallization of bcc α-Fe and the precipitation of Fe_2B compounds is not only determined by Cu and Nb addition but also decrease with increasing content. This put a further constraint on the alloy composition namely that boron content should be kept at a low or moderate level in order to obtain an optimum nanoscaled structure. Amorphous alloys provide an extremely convenient precursor material for preparation of nanocrystals through the crystallization process controlled by thermal treatments [1.4 -1. 7]. Müller *et. al*. [1.8] studied the influence of Cu/ Nb content and annealing condition on the microstructure and the magnetic properties of FINEMET alloys. Grain size, phase composition and transition temperature were observed to depend on the Cu/ Nb content. These represent a new family of excellent soft magnetic core materials and have stimulated an enormous research activity due to their potential applications [1.9 – 1.11]. Investigations have been carried out on the effect of substitution of Au for Cu in the FINEMET on the crystallization behavior and magnetic properties [1.12]. It has been found that Au behaves similarly as Cu on crystallization behavior and magnetic properties. Saturation magnetization on of the large number of metallic characteristic need to be studied for the understanding of the metallic system [1.13 – 1.14].

As known, controlled annealing of amorphous ribbons leads to the new materials with a nanocrystalline structure which have excellent soft magnetic

properties for example an enhanced permeability and very low power losses. The theoretical understanding of the nanometric grain with magnetic softness has been consolidated in the light of random anisotropy model (RAM) as proposed by Alben *et. al.* [1.15]. On the basis RAM showed that extraordinary soft magnetic properties of nanocrystalline materials arise due to strong intergranular magnetic coupling, the suppression of effective magnetocrystalline anisotropy and vanishing magnetostriction. The magnetocrystalline anisotropy vanishes when the grain size is smaller than the ferromagnetic exchange length and magnetostriction goes towards zero due to the cancellation of the positive magnetostriction of α -Fe(Si) grains and negative magnetostriction of the amorphous matrix. The aim of the present work is to study phase to the remaining amorphous and nanocrystalline phase, where the remaining amorphous phase crystallites increased significantly compared with crystallization temperature of the Cu-free alloy. The quantity of nanocrystalline phase which can be formed at given temperature depends on the FINEMET alloy in which Cu replaced by Ag. The microstructural evolution by the crystallization of $Fe_{72.5}Ag_2Nb_3Si_{13.5}B_9$ melt spun amorphous ribbons will be investigated. Not only the promising technological application but also the coexistence of various magnetic phases at elevated thermal treatment temperature makes these attractive for studying basic magnetic phenomena.

1.2 The Aim and Objectives of the Present Work

The main objective of the research work is to investigate nanocrystalline formation in $Fe_{72.5}Ag_2Nb_3Si_{13.5}B_9$ metallic ribbon and to study the phase constitution and the magnetic properties. That's find out the optimum composition and grain distribution affecting the magnetic properties of the system.

The objectives of the research work as follows:

- To synthesize of the FINEMET alloys in the form of the ribbon with replacement Cu with Ag in amorphous state by rapid solidification technique.
- To study the growth nanocrystals on amorphous matrix by thermal treatment.
- To study the formation nanocrystals grain size distribution as affected by heat treatment with varying temperature and holding time will be studied by X-ray diffraction (XRD).
- To study the optimization of annealing temperature corresponding to the magnetization of this nanocrystalline ribbon.

- To study of Correlation of the evaluation of nanograins with the magnetic properties.

1.3 Experimental Reason for Choosing this Research Work

In the present work, soft magnetic amorphous FINEMET type alloy nominal composition of $Fe_{72.5}Ag_2Nb_3Si_{13.5}B_9$ synthesized by a melt spinning technique. To improve the magnetic properties of this amorphous ribbon, microstructure is an important parameter that can be controlled by heat treatment condition. Also one effective way of preparing nanocrystalline alloy via the amorphous state of material is an appropriate heat treatment that has been found leading to crystallization phase.
The experimental methods that would be used in this research work are follows:

- Amorphousity of the samples will be checked by X-ray diffraction (XRD).
- Differential thermal analysis (DTA) will be used to evaluate the phase transformation and to determine the crystallization temperature. From the DTA analysis evaluation of the crystallization activation energy of various phases will be done.
- All the annealing heat treatment will be performed in evacuated alumina tube in configuration with a microprocessor controlled muffle furnace.
- Crystalline phase of the grains will be determined by XRD on samples annealed at different temperatures.
- Temperature and field dependence magnetization measurements will be performed using vibrating sample magnetometer (VSM).

The main study of the present work is Cu replaced by Ag substituted Fe-based nanocrystalline alloys of the above mentioned composition in the amorphous phase by using rapid solidification technique and their magnetic properties with the evolution of different phases by varying annealing temperature. The experimental results will be analyzed and interpreted. Finally it is shown how this material of this kind may be realized technologically and that its magnetic behavior corresponds entirely to the prediction of the theory. The accumulated results would be interpreted on the basis of existing theories of magnetism.

1.4 Application of Nanocrystalline Ribbons

The key beneficial feature of amorphous alloys lied in their low losses but this was at the price of lower induction. The standard for power devices applications that were considered included power transformers, magnetic shields, acoustic delay lines, tensile stress transducers and transverse filters. The properties of amorphous magnetic alloys with respect to application in electronics, in particular saturation inductors, permeabilities, hysteretic and eddy current losses and magneto electric properties were considered. Application for amorphous magnets that were suggested included

(i) 400 Hz power transformers
(ii) Inductive components for switch mode power supplies
(iii) Magnetic shields
(iv) Magneto-electric transducers
(v) Magnetic heads for data storage applications and
(vi) Magnetic springs

Materials requirements for conventional magnetic heads include: (a) large permeabilities (b) large saturation inductions (c) large electrical resistivities, mechanical hardness and wear resistance.

The attenuation of pulse voltage in choke coils was improved using FINEMET cores as compared with Fe-based amorphous materials. These choke coils can be used over a wide frequency range as well as for protection from high voltage noise caused by lightning. Soft magnetic properties require that nanocrystalline grains be exchange coupled and therefore any of the processing routes based on power production must be coupled with a compaction method in which the magnetic nanoparticles end up exchange coupled. Nanocrystallization of amorphous precursors will also require compaction to produce shapes and to improve mechanical properties, as ribbons are quite brittle after nanocrystallization. The soft magnetic properties required for rotor applications in the more electric aircraft are in some senseless restrictive than those for the applications of FINEMET. The attractive technical characteristic of nanocrystalline alloys has no microstructural discontinuities such as dislocations, grain boundaries as or precipitates. This significantly reduces the possible pinning sites for domain walls, reducing the coercivity. The absence of microstructural

discontinuities resulted in improved corrosion resistance. The highly elastic behavior of these alloys makes them less prone to degradation during handling.

1.5 Review of Researches on FINEMET

Amorphous materials based on Fe-Si-B show good magnetic properties when they are heat treatment below their crystallization temperature. While the Fe-Cu-Nb-Si-B alloys exhibit extraordinary high permeability, two orders of magnitude higher their conventional Fe-Si-B alloys due to heat treatment just above the crystallization temperature for a specific time. The great scope of technical application of this material $Fe_{73.5}Cu_1Nb_3Si_{13.5}B_9$ arises from this freedom of tailoring the magnetic properties [1.16 - 1.17].

The study of Yoshizawa *et. al.* [1.18] and Noh *et. al.* [1.19] on the role of nucleating agent Cu on the crystallization behavior of the composition $Fe_{73.5}Cu_1Nb_3Si_{13.5}B_9$ revealed that the average grain size is relatively large at crystallization temperature due to lower crystallization rate with no addition of Cu and annealing of this Cu free alloy leads to simultaneous or sequential formation of several crystalline phases. Kataoka *et. al*. [1.20] verified the role of Au in place of Cu and reported that Au is the only element, which has a comparable effect on the crystallization behavior.

Each cluster formation causes a concentration fluctuation of Fe also, since Cu substitutes for iron. Because of this concentration fluctuation, the density for the nuclei of the bcc crystalline phase is increased significantly although the evidence of concentration fluctuation in the fully amorphous state has not been observed because the investigation [1.21] observed the Cu cluster and bcc phase simultaneously at the early stage of the nanocrystallization. The consequence is an extremely fine nucleation of bcc Fe-Si crystallites at a high rate, which subsequently grow in a diffusion controlled process as the annealing proceeds further [1.22].

Suzuki et. al. [1.23], Alben *et. al.* [1.24] and Sawa *et. al.* [1.25] worked on the relation of grain size and domain wall width. If the grain size exceeds the domain wall width, domains can be formed within the grains and the coercive field, H_c is found to depend on the grain size D_g as $H_c \; \alpha \; D_g^6$.

Herzer [1.26] studied on Curie temperature and permeability of nanocrystalline material. According to him when measuring temperature approaches the Curie point

of the inter-granular amorphous phase, the exchange coupling between the crystallites is largely reduced. As a result, the initial permeability drops down. As reported by Hakim *et al.* [1.27] and S. Manjura Haque *et al.*[1.28], magnetic initial permeability of nanocrystalline amorphous ribbon strongly depends on annealing temperature and exhibits super paramagnetic behavior at $T > T_c^{am}$. When T_c^{am}, the grain coupling is largely but not interrupted above T_c^{am} and still persists to higher value of permeability compared to annealed temperature at T_c^{am} exhibiting the magnetic coupling between particles is significant. The precise coupling mechanism for this type of behavior at $T > T_c^{am}$ may be explained in terms of exchange penetration through thin paramagnetic inter-granular layer and/or dipolar interactions.

New phenomenon about surface morphological study has been studied by O. Životský · L. Klimša, A. Hendrych, Y. Jirásková and J. Buršík [1.29]. They observed that yield formation of small α-FeSi nanocrystals of approximately (5 - 10) nm in dimension embedded in an amorphous matrix. Just such a surface microstructure causes asymmetric hysteresis loops measured by MOKE at different places at the ribbon surface.

Investigation of the effect of substituting Mn for Fe on the crystallization kinetics of amorphous $Fe_{73.5-x}Mn_xCu_1Nb_3Si_{13.5}B_9$ (x = 1, 3, 5, 7) alloys had taken by N. Bayri and his team. The samples were annealed at 550^{o}C and 600^{o}C for 1 h under an argon atmosphere. The X-ray diffraction analyses showed only a crystalline peak belonging to the α -Fe(Si) phase, with the grain size ranging from 12.2 nm for x = 0 to 16.7 nm for x = 7.The activation energies of the alloys were calculated using Kissinger, Ozawa and Augis–Bennett modelsbased on differential thermal analysis data [1.30].

Hakim et. al. [1.31] studied that the amorphous ribbons of composition $Fe_{77}Cu_{0.6}Nb_{2.4}Si_{11}B_9$ have been annealed at threeannealing temperatures of 500°C, 520°C and 530°C for 1 hour, which produces homogeneous, ultra-fine grain structure of about 11 nm on an average. The amorphosity of the ribbons has been confirmed by x-ray diffraction. Activation energy of crystallization of α- Fe(Si) and iron boride phase has been obtained as 2.02 eV and 3.66 eV respectively.

Replacement of Ag for Cu in the FINEMET with composition $Fe_{72.5}Ag_2Nb_3Si_{13.5}B_9$ alloy on the crystallization behavior and magnetic properties is observed. In these materials it has been determined that an important averaging of the nanocrystalline anisotropy over many grains coupled within an exchange length is at

the root of magnetic softness of these materials. The crystallization kinetics and chemical partitioning occurring during crystallization will be described essentially. The effect of replacement Ag for Cu in FINEMET nanograin structure and thermal stability of the alloy draws much interest for the present research from the view point of applications.

1.6 Organization of the Thesis

The thesis has been divided into five chapters.

Chapter I: general introduction followed by The aim and objectives of the present work, reason for choosing this research work, application of nanocrystalline ribbons, review of researches on FINEMET and organization of the thesis.

Chapter II: the preparation procedures of the nanocrystalline alloys are described. In **Chapter III:** the theoretical background of the stability of amorphous alloys, theories of magnetization are discussed and the experimental details including Differential Thermal Analysis (DTA), X-ray Diffraction (XRD) analysis, and Vibrating Sample Magnetometer (VSM) are described.

In Chapter IV: the details results regarding DTA, activation energy, corresponding crystallization temperature, XRD method after heat treatment of the sample at different temperatures, Lattice parameter, Silicon content, Grain size determination, field dependence of specific magnetization and annealing effects on saturation specific magnetization are discussed.

Chapter V: contains conclusion, achievement of works and further suggestion of this work.

Finally a complete list of reference has been given towards the end of the chapters.

THEORETICAL BACKGROUND

2.1 Composition of the Nanocrystalline Alloy

Nanocrystalline amorphous material ribbons can be considered as an off-shoot of amorphous materials. In fact nanocrystalline amorphous ribbons are composite materials where nanocrystals are embedded in an amorphous matrix. Nanocrystalline materials represent one of the most active research areas in recent time for the atomic tailoring of materials with specific properties and property combinations. However, it is still in its infancy since its emergence as potential materials has just begun at this stage of development.

Generally the optimum mechanical and magnetic properties of nanocrystalline soft magnetic materials are obtained for partially crystallized materials. This means that those materials are formed in two phases [2.1]. In general nanocrystalline alloys can be described as $TL_{1-x}(TE, M, NM)_x$ where

- TL denotes a late ferromagnetic transition metal element (TL= Co, Ni or Fe)
- TE denotes an early transition metal element (TE = Zr, Nb, Hf,Ta etc.)
- M is metalloid (M = B, P, Si, etc.) and
- NM is a noble metal (NM = Cu, Ag, Au etc.)

This composition usually has $x < 0.02$ i.e. with as much late ferromagnetic transition metal (TL of Fe, Co or Ni) as possible. The remaining early transition metals (TE = Zr, Nb, Hf, Ta, etc.) and metalloids (B, P, Si, etc.) are added to promote glass formation in the precursor. The noble metal elements (NM = Cu, Ag, Au, etc.) serve as nucleating agents for the ferromagnetic nanocrystalline phase. The compositions are limited by where glass formation can occur prior to the nanocrystallization route. These alloys may be single phase (Type-I) but are generally two phase materials with a nanocrystalline ferromagnetic phase and a residual amorphous phase at the grain boundaries (Type-II).The type-II nanocrystalline alloys might have general properties:

- Relatively high resistivity (50-80μΩ-cm)
- Low magneto crystalline anisotropy and
- Increase mechanical strength

With properties such as these, nanocrystalline alloys have great potential as soft magnetic properties. In the ongoing research we are any interested about the type-II.

One of the important features of this magnetic system is that one can play with different compositions, annealing temperatures and time to control the grain size and their distribution upon, which the magnetic properties of these new materials strongly depend. In choosing the composition, one has to consider the magnetic component like Fe, Co of Ni, the crystallization initiating component e.g. Cu and the component Nb for stabilizing the nanocrystal by inhibiting the grain growth and glass forming materials like Si, B, etc.

Nanocrystalline soft magnetic alloys have received considerable attention due to their excellent soft magnetic properties [2.2]. Small addition of Nb into Fe-Si-B amorphous materials charges considerable their crystallization process, which is executed under appropriately controlled conditions and the specific purpose of these addition are

- The element is used for helping the formation of nuclei and ultra-fine grain and
- The element is used to impede the growth of the crystallites.

In this material, the nanocrystalline state is composed of a fine structure of α-Fe (Si) and is usually around 10nm. For such as average grain size the exchange interaction dominates the magnetic behavior of randomly oriented crystallites guided by random anisotropy [2.3]. In the present thesis work nanocrystalline alloy is prepared by substitution of Cu by Ag of FINEMET with composition $Fe_{72.5}Ag_2Nb_3Si_{13.5}B_9$.

2.1.1 An overview of Nanocrystalline Materials

This is not necessarily the case for multiphase system such as find in many of the nanocrystalline alloys that are produced from amorphous precursors. For a two phase microstructures with a ferromagnetic inter granular amorphous phase and a single ferromagnetic nanocrystalline phase, the nature of the nanocrystal-amorphous-nanocrystal coupling is of the paramount importance to the properties of these materials. This coupling depends upon the size of the nanocrystallites, and more importantly upon the amount, chemistry and thickness of the amorphous phase. The best properties, of course, are when both criteria are met, below presumably the lower Curie temperature of the amorphous phase.

Slawska-Waniewska *et. al.* [2.4] have observed T-dependent magnetic response in partially and fully nanocrystallized FINEMET materials. They concluded

that for sufficiently small nanocrystals with enough inter granular material between them to diminish or destroy coupling between grains that super paramagnetic response would be observed. This would not be the case for properly annealed samples with sufficient volume fraction of the nanocrystalline ferromagnetic. Characteristic of super paramagnetic response, first proposed by Bean *et. al*. [2.5] includes:

(i) a Langevin function scaling of magnetization data

(ii) disappearance of the coercivity above a blocking temperature and time dependent magnetization, due to thermally activated switching of the magnetization.

Nanocrystalline amorphous ribbon can be considered as an off-shoot of amorphous materials. In fact nanocrystalline amorphous ribbon is a composite material where nanocrystals are embedded in an amorphous matrix. Nanocrystalline materials represent one of the most active research areas in recent times for the atomic tailoring of materials with specific properties and property combinations**.** In addition to the understanding of the usual properties possessed by nanophase materials, there are three other associated areas, which need serious attention:

(i) Identification and development of suitable preparation methods, especially those which are capable of providing large industrial quantities of nanometer scale materials.

(ii) Development of processing methods for manufacturing these materials into useful size and shapes without losing their desirable nanometer size feature and

(iii) Identification of proper characterization methods, where the nanometer size range of these materials falls just below or at the resolution limit of the conventional tools.

2.2 Alloy Design Issues

Alloy design issues include issues of chemistry and processing designed to:

(i) Optimize one of a number of important intrinsic and or extrinsic magnetic properties and

(ii) Optimize structural or microstructural features which promote important magnetic properties.

The first of these issues concerns the choice of chemistry so as to impact the intrinsic magnetization of the material. The second issue pertinent to alloy additions designed at aiding formation of an amorphous phase.

Microstructure of alloy in influence extrinsic magnetic properties, the important microstructure features should be recognized including grain size, shape and orientation, defect concentration, compositional in homogeneities, magnetic domain and domain wall. The development of soft magnetic materials for application requires attention to a variety of intrinsic magnetic properties as well as development extrinsic magnetic properties though an appropriate optimization of the microstructure.

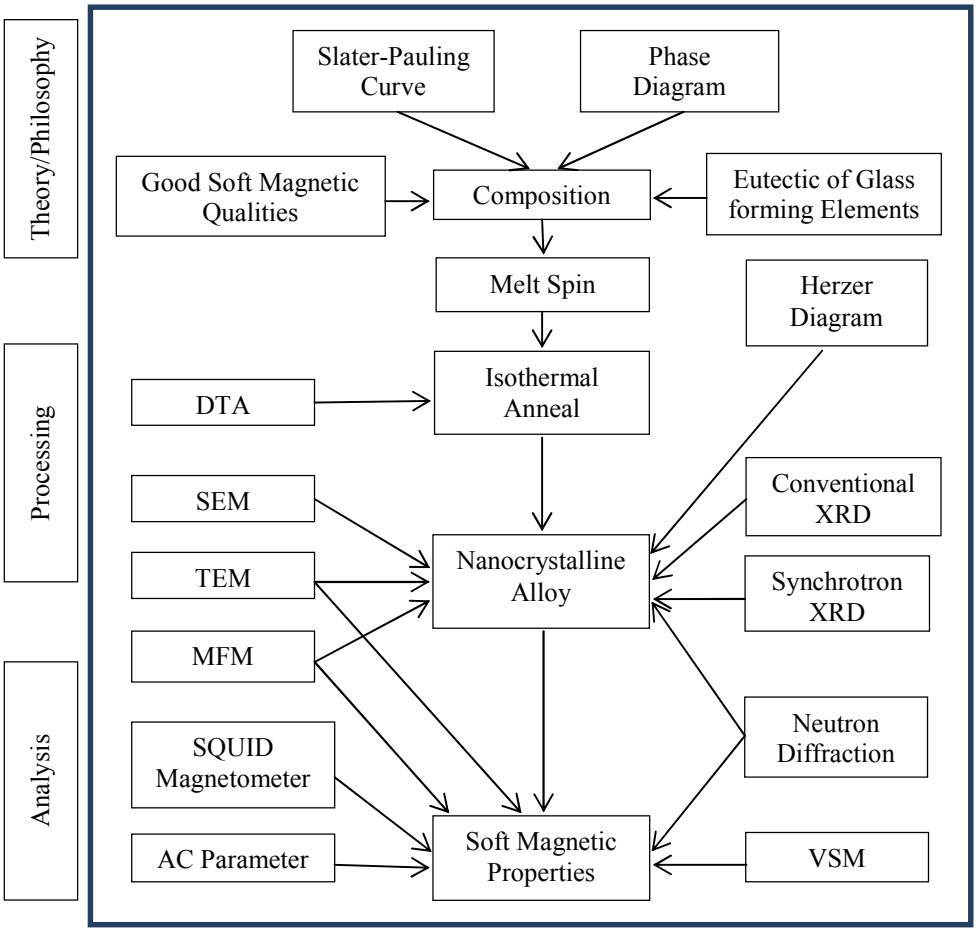

Figure 2.1 : Flowchart for the consideration in designing and developing nanocrystalline soft magnetic material from an amorphous precursor route

Alloy design issue are in many was influenced by processing routes used to achieve desired microstructures. In Figure 2.1 illustrates a flowchart for the considerations in designing and developing nanocrystalline soft magnetic material

from an amorphous precursor route as an example of the design process. Here we consider first, the effects of alloy composition on intrinsic magnetic properties. This is followed by consideration of alloying additions necessary to produce an appropriate amorphous precursor. Typical experimental steps used to identify the structure and properties of the resulting materials are also illustrated.

2.2.1 Formation of Nanocrystalline Stage

The formation of the particular nanocrystalline structure is essentially related to the combined addition of Cu and Nb (or other group IV or VI elements) and their low solubility in Fe-Si (< 0.2 at % Cu, < 0.1 at % Nb). Cu enhances the nucleation of bcc grains while Nb impedes grain coarsening and at the same time, inhibits the formation of Boride compounds. The evolution of microstructure during annealing is depicted schematically in Figure 2.2 and summarized as follows according to Hono *et. al.*[2.6 - 2.7].Formation of the nanocrystalline microstructure in the amorphous phase was depicted by G. Herzer in 'the nanocrystalline soft magnetic alloys' [2.8].

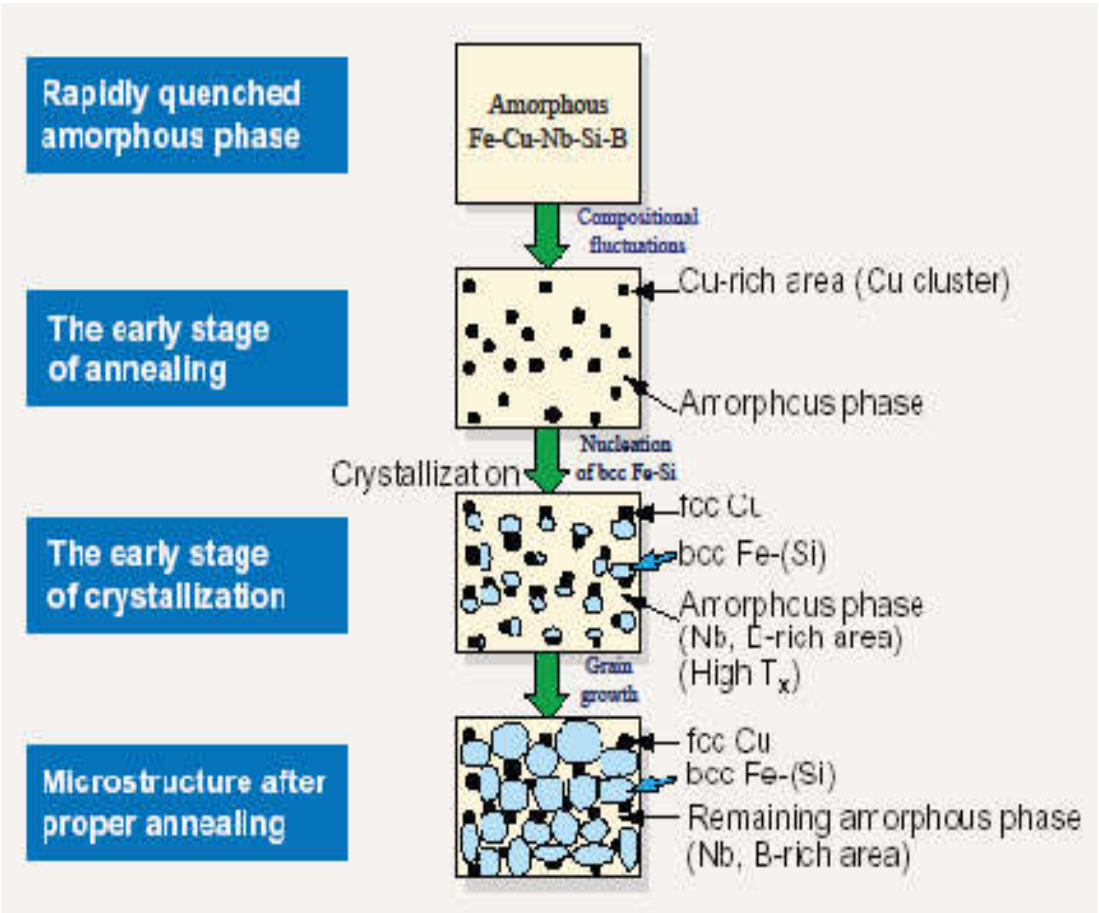

Figure 2.2 : Schematic illustration of the formation of nanocrystalline structure

The nanocrystalline microstructure and the accompanying soft magnetic properties are rather insensitive to the precise annealing conditions within a wide range of annealing temperature $T_a \approx 550 - 600^oC$. They develop in a relatively short period of time and do not much latter even after prolonged heat treatment of several hours [2.9]. A typical heat treatment like $T_a \approx 580^oC$ in most cases yields a nanocrystalline microstructure to the Quasi-equilibrium state and characteristic for the individual alloy composition.

Thus the regions in between the Cu replacement Ag- rich clusters provide a significantly increased density of nucleation sites for the crystallization of bcc Fe. The consequence is an extremely fine nucleation of bcc Fe-Si crystallites at a high rate, which subsequently grow in a diffusion-controlled process as the annealing proceeds furthers. As annealing goes on the grain size of the α-Fe(Si) increases. At the same time the Si content of this phase keeps increasing since Si tends to be partitioned to the bcc α-Fe(Si) phase. Since the Nb and B enrichment in the amorphous phase stabilizes the remaining state, the grain growth of the bcc phase eventually stops.

At the optimum stage, three distinct phases are present based on the chemical composition. As the bcc Fe-Si phase forms, Nb and B are excluded from the crystallite because of their low solubility in bcc Fe and are enriched in the residual amorphous matrix. At a time all the Si tends effectively to be partitioned into the bcc Fe-Si phase [2.10-2.11]. The particular enrichment with B and Nb increasingly stabilizes the residual amorphous matrix, thus, hinders coarsening of the bcc grains. The presence of Nb at the time inhibits the formation of Fe_2B compounds. The transformation finally ceases in a metastable two-phase microstructure of bcc Fe-Si embedded in an amorphous Fe-Nb-B matrix.

2.2.2 Advantages of Soft Nanocrystalline Alloys

Nanocrystalline amorphous ribbons are produced by the melt-spinning technique to produce an amorphous metal and then heat treating this alloy at temperature higher than its crystallization temperature. The choice of soft magnetic materials for applications has been guided by recent developments in the field of soft magnetic materials. Amorphous and nanocrystalline magnetic materials, in terms of combined induction and permeability are now competitive with Fe-Si bulk alloys and the Fe-Co alloys. In Figure 2.3[2.12], figures of merit for Fe-based amorphous alloys, Co-based amorphous alloys and nanocrystalline alloys are summarized. Co-based

amorphous alloys, Fe-based amorphous alloys and nanocrystalline alloys have evolved over the past decades with soft magnetic properties which now exceed those of the bulk alloys based on Fe, Co and Fe-Co.

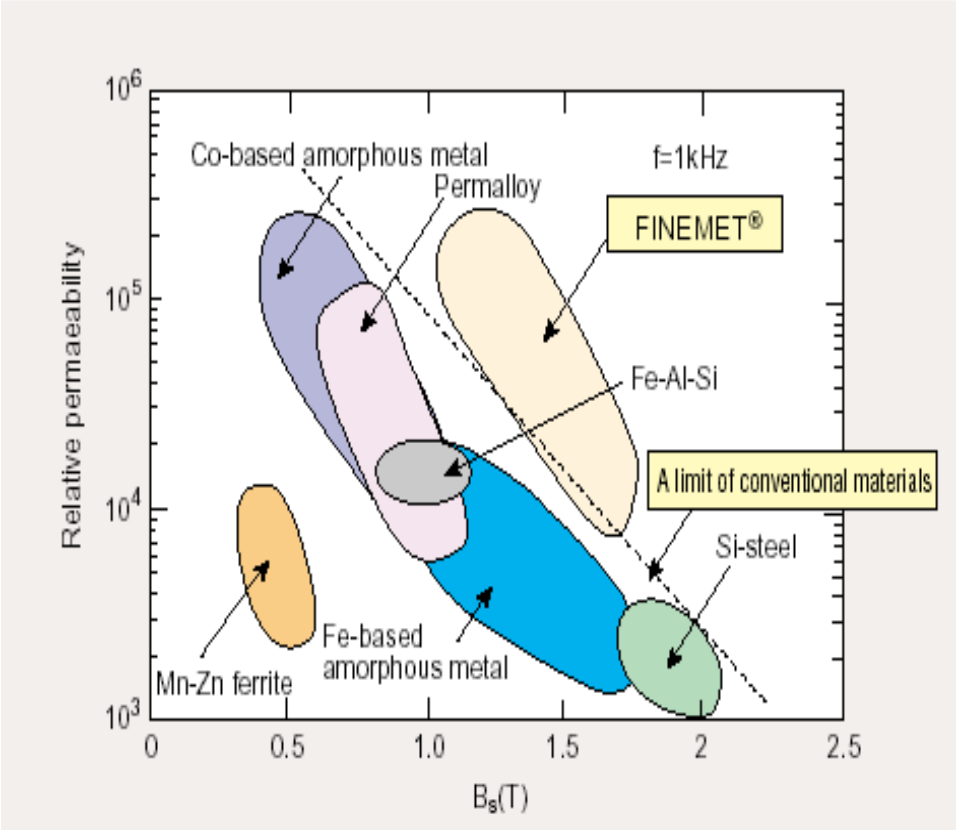

Figure 2.3 : FINEMET is superior compared to conventional materials

This FINEMET material is still in its immaturity since its emergence, although much research work has been carried out for the potential utility of this unique material.

At the stage of development, this material has the following advantages:

- High saturation magnetic flux density more than 1 Tesla or 10 kOe.
- High permeability over $\mu_i \approx 10{,}000$ at 100 kHz.
- Excellent temperature characteristics.
- Less affected by mechanical stress.
- Audio noise emission is very low, lower magnetostriction significantly reduces audible noise emission when the voltage and current is applied to the core at audible frequency range.

- Flexible to control the magnetic properties, "B-H curve shape" during the annealing, and three types of B-H curve squareness, high, middle and ion resonance ratio, corresponding to various application.

2.2.3 Conditions for the Formation of Nanocrystalline Alloys

The essential conditions for preparing of nanocrystalline materials are:

(i) The magnetic properties are highly dependent on the grain size; if the grain size is larger; the magnetic anisotropy would be very high, which is turn will have diverse effect on the soft magnetic properties specially the permeability.

(ii) For the crystallization process there should be nucleation centers initiated to be distributed throughout the bulk of amorphous matrix.

(iii) For stabilizing the crystallites there must be a nucleation.

(iv) Nanocrystalline materials obtain from crystallization must be controlled that crystallites do not grow too big. The grain growth should be controlled so that the grain diameter is within 15-20nm.

(v) The size of the grain can be limited to nanometer scale by doping group-II metals are

→ Cu (Au , Ag, ……)

→ Nb, W, Mo, Cr, Ta etc.

(vi) The stability must be lower and the crystallization must be higher.

In addition to the understanding of the unusual properties possessed by nanophase materials; there are three other associated areas, which need serious attention:

- Identification and development of suitable preparation methods, especially which are capable of providing large industrial quantities of nanometer scale.
- For manufacturing of these materials processing methods should be develop useful size and shape without losing their nanometer size feature.
- Identification of proper crystallization methods, where the nanometer size range of these materials falls just below or at the resolution limit of the conventional tools.

2.3 Amorphous Alloys or Metallic Glass

An amorphous (from the Greek a, without, *morphe*, shape, form) or non-crystalline solid is a solid that lacks the long-range order characteristics of a crystal. In part of the older literature, the term has been used synonymously with glass. The total structure in amorphous metallic material is distinct from that of window glass. The term amorphous defines a non-crystalline body while a glass refers to a molten mass that is cooled rapidly to prevent crystallization. By analogy, the term 'metallicglass' usually refers to a metallic alloy rapidly quenched in order to freeze its structure from the liquid state. The expression 'glass' in its original sense refers to an amorphous or nanocrystalline solid formed by the continuous cooling of liquid while a solid is defined somewhat arbitrary as object having a viscosity greater than 10^4 Pa.s [2.13]. Glasses have been found in every category of materials and of various bond types, Covalent, ionic, Vender Walls, hydrogen and metallic. Different types of amorphous solids include gels, thin films and nanostructured materials.

2.3.1 Stability of the Amorphous and Nanocrystalline Materials

Amorphous materials are always metastable state which leads to transform into more stable crystalline phase. There are three kinds of stability of significance for magnetic ribbons;

(i) Their resistance to the initiation of crystallization.

(ii) Structural relaxation effect, and

(iii) The relaxation or reorientation of directional order.

Controlled crystallization seems from the amorphous state to be the only method presently available to synthesize nanocrystalline alloys with attractive soft magnetic properties. The formation and the resultant stability of amorphous alloys are important topic both for theoretical understanding and technically. The theoretical analyses of the factors controlling the case of formation and the stability of the resultant amorphous alloys have been extensively reviewed [2.14 – 2.15]. From the thermodynamic view point [2.16 – 2.17], the ability of an alloy to be quenched into the glassy state is generally measured by the magnitude of the quantity.

$$\Delta T_g = T_m - T_g \qquad (2.1)$$

Where T_m and T_g are the melting and glass temperature respectively. The stability of the glass after formation in a similar manner is generally measured by the magnitude of the quantity.

$$\Delta T_x = T_x - T_g \qquad (2.2)$$

Where T_x is the temperature for the onset of crystallization. As the temperature decrease from T_m, the rate of crystallization will increase rapidly but then fall rapidly as the temperature decrease below T_g. So that if we quenched a molten alloy rapidly enough to temperature below T_g a quasi-equilibrium amorphous phase is obtained. There is no direct relation between the easy of formation and the resultant stability of an amorphous alloy. The amorphous alloy composition most favorable for glass formation is near eutectic i.e. the composition in which the transformation from the liquid state to solid state takes place instantaneously without passing through liquid plus solid mixed phase. The deeper the eutectic the better is the glass formation ability [2.18]. There have been three approaches for relating the stability of the glass, i.e. its microstructure:

(i) Barnal's model of randomly packed hard sphere's [2.19]. The atoms of the metal are assumed to from a random network of close packed hard spheres and the smaller metalloid atoms fill the holes inherent in such structure.

(ii) The effect of atomic sizes and inter atomic interactions [2.20], i.e. chemical bonding suggested that it is chemical bonds which are dominating factors in glass formation and stability.

(iii) The third approach [2.21] is based on the role of the electron gas and showed that under certain circumstances a nearly free electron gas will produce a barrier against crystallization.

The transition to the glassy state and the crystalline state is accompanied by an exothermic heat effect giving rise to a sharp peak in temperature dependence of the heat flow. Therefore, DTA is a widely used technique to study thermally induced transformations in amorphous alloys and to determine T_g and T_x. The magnitude of T_g and T_x are very different for amorphous materials and depend strongly on composition. The activation energy ranges typically between 2 and 6 eV [2.22].

2.3.2 Characteristics of the Glass Transition Temperature

When the time scale of molecular rearrangements occurs glass transition temperature (T_g) are too long for equilibrium to be maintained:

(i) T_g means the time scale of the experiment maters.

(ii) A high frequency/short time scale experiment allows less long for equilibrium to be established – even for an identical cooling rate.

(iii) NMR (high frequency technique 10^{15} Hz.) always measures a higher T_g than DTA (1 Hz.).

(iv) In the glass itself, entropy is similar to the crystal and original in vibrational modes, which are still present.

(v) Long range transitional motions are frozen out. The temperature T_g configuration relaxation (including translational motion) but vibrational relaxations are still in equilibrium.

(vi) T_g decreases as melt cooled more and more slowly.

(vii) When the timescale of the experiment and the configuration relaxation time coincide, begin to see departure from equilibrium.

(viii) The time scale for configuration relaxation will be related to rotational or translational diffusion coefficient.

(ix) Optional definition of T_g is when the viscosity of the super-cooled liquid exceeds 10^{13} NSm^{-2}. Whereas in the liquid there is an Arrhenius type with a Boltzmann factor containing activation energy.

2.4 Differential Thermal Analysis and its Application

Differential thermal Analysis (DTA) is an important technique for the study of structural change both in solid and liquid materials under heat treatment. During this process, the temperature difference between a substance and reference material is measured as a function of temperature whilst the subject and the reference material are subjected to some controlled temperature program. The transition of an amorphous or glassy state to crystalline state is accompanied by an exothermic heat effect that gives rise to a sharp peak in temperature dependence of the heat flow. To study this thermally induced transformation in amorphous alloys, DTA is a widely used technique. Amorphous alloys are in a metastable state and tend to transition into stable crystalline phases. At temperature below the crystallization temperature, structural relaxation effect takes place which are caused by atomic rearrangements.

DTA is an important technique for the study of structural change both in solid and liquid materials under heat treatment. The principle of DTA is widely used to understand the crystallization nature of the amorphous. Differential thermal analysis is a direct and effective technique for analyzing the kinetics of amorphous materials and stability with respect to crystallization process.

The crystallization is associated with the nucleation and growth process. Since the formation of an amorphous alloy depends on the absence of LRO, change of composition is expected to affect T_g and T_x. This is because long range ordering of atoms depends on the free energy difference between the crystalline state and the amorphous state. The magnitude of T_g and T_x are very different for amorphous materials and depend strongly on composition. Using DTA technique it is possible to determine T_g and T_x. Nanocrystalline amorphous ribbons prepared by rapid quenching method have been subjected to DTA using a Shima dzu Thermal Analyzer. Different peaks, crystallization temperatures, crystallization activation energies are obtained from this analysis.

2.4.1 Evaluation of Activation Energy Based on DTA Technique

Based on the work of Murray and White [2.23 – 2.25], the kinetics of materials can be understood by interpretation of DTA patterns of the materials. The dependence of T_x on the heating rate $\beta = \frac{dT}{dt}$ can be used to determine the activation energy of crystallization [2.26]. Considering the fraction x of amorphous material transformed into the crystalline state in time t and at temperature T obtains for the first-order rate process [2.27 – 2.28]

$$\left(\frac{\delta x}{\delta t}\right)_T = K(1-x) \tag{2.3}$$

For thermally activated process, the rate constant K obeys an Arrhenivs type of equations

$$K = K_o e^{-\left(\frac{\Delta E}{RT}\right)} \tag{2.4}$$

where K_o is a constant and ΔE is the activation energy. Combining equation (2.3) and (2.4) and using $dx = \left(\frac{\delta x}{\delta t}\right)_T dt + \left(\frac{\delta x}{\delta t}\right)_t dT$ with $\left(\frac{\delta x}{\delta t}\right) dt \cong 0$, are obtains

$$\frac{dx}{dt} = K_o(1-x)e^{-\left(\frac{\Delta E}{RT}\right)} \tag{2.5}$$

$$\frac{d^2x}{dt^2} = \frac{d}{dt}\left[K_o(1-x)e^{-\left(\frac{\Delta E}{RT}\right)}\right]$$

$$= -K_o\frac{dx}{dt}e^{-\left(\frac{\Delta E}{RT}\right)} + K_o(1-x)\frac{d}{dT}\left\{e^{-\left(\frac{\Delta E}{RT}\right)}\right\}\frac{dT}{dt}$$

$$= -K_o\frac{dx}{dt}e^{-\left(\frac{\Delta E}{RT}\right)} + \frac{dx}{dt}\left(\frac{\Delta E}{RT^2}\right)\beta$$

At the peak of the exothermic heat, the change of the reaction rate $\frac{d^2x}{dt^2} = 0$, yielding with T=T_x but $\frac{dx}{dt} \neq 0$

$$K_o e^{-\left(\frac{\Delta E}{RT_x}\right)} = \left(\frac{\Delta E}{RT_x{}^2}\right)\beta \qquad (2.6)$$

From equatio (2.6) it is easily seen that

$$\frac{d\left(ln\frac{\beta}{T_x^2}\right)}{d\left(\frac{1}{T_x}\right)} = -\frac{\Delta E}{R} \qquad (2.7)$$

Here $\beta = \frac{dT}{dt}$ the heating rate. ΔT_x for the stability of amorphous alloys as given by equation (2.2) and is obtained from DTA. Similar correlation between thermal stability as measured by ΔT_x and ΔE appears too small.

From the measured data of the heating rate (β) and the respective crystallization temperature (ΔT_x), the activation energy can be deduced from the slope of a plot $ln\frac{\beta}{T_x^2}$ versus $\frac{1}{T_x}$ from equation (2.7) can be derived from transformation theory, where ΔE is the activation energy for versus flow and other terms have been omitted because they an insignificant temperature dependence in this region of temperature. The values of ΔE also appear to correlate well with the number of atomic species in the alloy; the more complex the alloy the grater is ΔE.

2.5 Determination of Nanometric Grain Size by X-Ray Diffraction

Nanocrystalline alloys are basically crystalline and because of their crystallinity and they exhibit Bragg scattering peaks in X-ray diffraction experiments. However, due to their small size, significant fine particle broadening is observed in the Bragg peaks. The X-ray scattering from a crystalline solid is given by Bragg's law:

$$2d\sin\theta = n\lambda \qquad (2.8)$$

This equates the path difference scattered from parallel crystalline planes spaced d = d_{hkl} apart to an integral number (n) of X-Ray wavelength λ. Here θ is the X-Ray angle of incidence (and of diffraction) measured with respect to the crystalline planes. Braggscattering occurs at discrete values of 2θ satisfying the Bragg condition for an infinite crystal, i.e. Bragg peaks are δ-functions. The peaks are broadened over a range of angles for finite sized crystals as shown in Figure 2.4 .

The better understand of the phenomenon of fine particle broadening following argument of Cullity [2.29] is outlined below. We consider a finite crystal of thickness, D_g = md, where is an integer and d is the distance between crystalline planes, i.e., there are m planes in D_g. considering Figure 2.4, if the broadened Bragg peak begins at an angle $2\theta_2$ and ends at $2\theta_1$, the breadth of the peak or full width at half maximum is given as:

$$\beta = \frac{1}{2}(2\theta_1\text{-}2\theta_2) = \theta_1\text{-}\theta_2 \qquad (2.9)$$

Now consider the path differences for each of the two angles $\theta_1$andθ_2, for X-rays travelling the full thickness of the crystal. The width β is usually measured in radians; intensity is equal to half the maximum intensity. As a rough measure of β , we can take half the difference between the two extreme angles at which the intensity is zero, which amounts to assuming that the diffraction line triangular in shape.

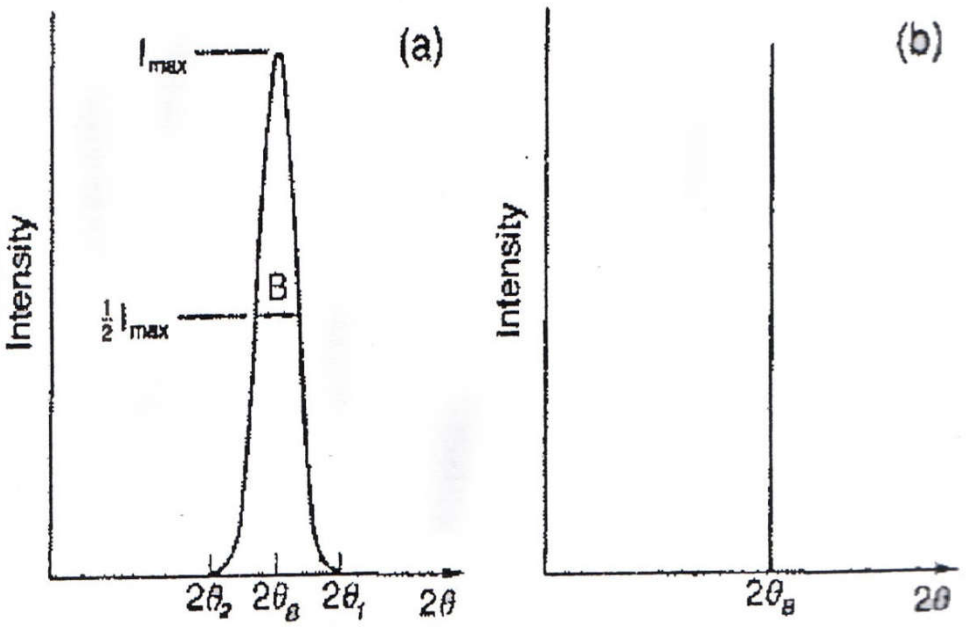

Figure 2.4 : Effect of fine particle broadening in XRD (a)fine particle and (b) perfect crystal

We now write the path difference equations for those two angles related to the entire thickness of the crystal rather to the distance between adjacent planes.

$$2D_g \sin\theta_1 = (m+1)\lambda \tag{2.10}$$

$$2D_g \sin\theta_2 = (m-1)\lambda \tag{2.11}$$

By the subtraction;

$$D_g (\sin\theta_1 - \sin\theta_2) = \lambda \tag{2.12}$$

$$2D_g \cos\left(\frac{\theta_1+\theta_2}{2}\right) \sin\left(\frac{\theta_1-\theta_2}{2}\right) = \lambda \tag{2.13}$$

But $\theta_1$and θ_2 are both very nearly equal to θ, so that $\theta_1 + \theta_2 \approx 2\theta$ and $\sin\left(\frac{\theta_1-\theta_2}{2}\right) \approx \left(\frac{\theta_1-\theta_2}{2}\right)$ thus the equation (2.13) can be written as:

$$2D_g \cos\theta.\left(\frac{\theta_1-\theta_2}{2}\right) = \lambda \tag{2.14}$$

From the equation (2.9) and equation (2.14) we get:

$$\beta.D_g\cos\theta = \lambda \tag{2.15}$$

$$D_g = \frac{\lambda}{\beta cos\theta} \tag{2.16}$$

A more exact empirical treatment yields:

$$D_g = \frac{0.9\lambda}{\beta cos\theta} \tag{2.17}$$

This is known as the Scherrer's formula. It is used to estimate the particle size of very small crystals from the measured width of their diffraction curves.

2.6 Magnetic Dipole Moments and Magnetization

Fe, Co or Ni, or the rare earth metal Gd as a majority component. The vast majority of soft magnetic materials have one or more of the ferromagnetic transition metal element. The magnetic dipole moments of the elemental and alloy magnets are almost completely understood through the Band Theory of Solids [2.30]. The band theory of solids considers the broadening of localized atomic states with discrete

Eigen values into a continuum of states for more itinerant electrons over arrange of energies. The theory allows for calculation of energy dispersion (i.e. energy as a function of wave vector) and orbital angular momentum specific and spin-resolved densities of states. The calculation of spin-resolved energy band and densities of states allows for the dispersion of atom resolved magnetic dipole moments, therefore spontaneous magnetization of element and alloy magnetic solids. Among the success of the band theory descriptions of magnetic properties are:

(i) The prediction of non-integral of half integral atomic dipole moments and resulting ground state magnetization in the metals and alloys.

(ii) The prediction that band widths and exchange splitting (energy differences between spin up and spin down bands) are intimately dependent on magnetic coordination number and atomic volume.

The variation of the mean atomic magnetic dipole moment as a function of composition in the transition metal alloys system. Spin resolved densities of states $g_+(E)$ and $g_-(E)$ for Co and Fe atoms, in an equiatomic Fe Co alloy, as a function of energy (where the Fermi energy, $E_F$is taken as the Zero of energy). The number of spin up, $n_+$and spin down, n_-electrons in each band can be calculated again by integrating these densities of state:

$$n_+ = \int_0^{E_F^+} g_+(E)dE \qquad (2.18)$$

and $$n_- = \int_0^{E_F^-} g_-(E)dE \qquad (2.19)$$

Here the Fermi energies, E_F, are the same and the zero's of energy are different for the two spin bands and the atom resolved (i.e. Fe and Co) magnetic dipole moments can be calculated as:

$$\mu_m = (n_+ - n_-)\mu_B \qquad (2.20)$$

Knowledge of atomic values or alloy density, then allows for the direct calculation of the alloy magnetization. The Fe-Co alloy, exhibits the largest magnetic inductions of any material, and also have T_c's which are desirable for high temperature applications. Fe rich alloys typically have smaller inductions and lower Curie temperatures than Fe-Co alloys. Co alloys can also be soft but only if the fcc phase of Co is present. Co rich alloys typically have smaller inductions and larger T_c's.

Table 2.1 : Spontaneous and room temperature magnetizations, magnetic dipole moments and Curie temperature for elemental ferromagnets

Element	$\mu_m@0K(\mu_B)$	$M_s@0K$ (G)	$M_s@RT$ (G)	$T_c(K)$
Fe	2.22	1740	1707	1043
Co	1.72	1446	1400	1388
Ni	0.606	510	485	627
Gd	7.63	2060	--	292
Dy	10.2	2920	--	88

Table 2.1, summarizes the absolute zero and room temperature (where applicable) magnetizations and atomic dipole moments for some important transition metal and rare earth elemental magnets. Also shown Curie temperatures i.e. ferromagnetic ordering temperatures which are not ground state properties that directly calculable from the band theory [2.31]

2.6.1 Magnetization of the Nanocrystalline Ribbon

The saturation magnetization of a material at a temperature of 0 K is one of its basic properties. Measurements are usually expressed as average moment per magnetic atom in units of the Bohr magnetron, μ_b as specific saturation magnetization for the amorphous alloy, $\sigma_s$in units for Am^2/kg. The moments of most amorphous alloys are lower than those of the structural disorder on the moments is very small.
These points out the importance of chemical instead of structural disorder. The reduction is least in B-based and highest in p-based glass. The observed moments on TM-M glasses can approximately fitted to a formula [2.32].

$$\mu = \left(\frac{\mu_{TM} C_{TM} - C_B - 2C_{sc} - 3C_\rho}{C_{Tm}} \right) \qquad (2.21)$$

Where μ_{TM} is the magnetic moment of TM-M atoms, taken as 2.6, 1.6 and 0.6 respectively in Bohr magneto for Fe, Co and Ni. C's are respective concentrations. This clearly demonstrates the change transfer from metalloid to d-band of transition metal and seems to suggest that 1, 2 or 3 electrons are transferred from each of B, Si (C, Ge) or P atom. The relative number of electrons donated can be listed as – $P_{13}C_7$> -$S_{15}B_{10}$> -$P_{16}B_6AI_3$>-$P_{14}B_{13}$>-B_{20} Based on the relative magnitudes of M_s.

2.6.2 Ferromagnetic ordering (Curie) Temperatures

Ferromagnetism is a collective phenomenon since individual atomic moments interact so as to promote alignment with one another. This collective interaction gives rise to the temperature dependence of the magnetization. Two models have explained the interaction between atomic moments. Mean Field Theory considers the existence of a non-local internal magnetic field, called the Weiss field, which acts to align magnetic dipole moments even in the absence of an applied field H_a. Heisenberg Exchange Theory considers a local (usually nearest neighbor) interaction between atomic moments (spins) which acts to align adjacent moments even in the absence of a field.

The basic assumption of the mean field theory is that this internal field is non-local and is directly proportional to the sample magnetization.

$$H_{INT} = \lambda_W M \tag{2.22}$$

Where the constant of proportionality, λ_W, is called the Weiss molecular field constant.

To consider ferromagnetic response in applied field, H_a, as well as the randomizing effects of temperature, we consider the superposition of the applied and internal magnetic fields. By analogy with the problem of paramagnetic moments, the average atomic dipole moment can be expressed in terms of the Brillouin function

$$<\mu_m> = \mu_m^{atom} B_J(\alpha') \tag{2.23}$$

Where $\alpha' = -\left(\frac{\mu_0 \mu_m^{atom}}{K_B T}\right)(H + \lambda_W M)$ for a collection of classical dipole moments. The saturation magnetization

$$M_S = N_m <\mu_m^{atom}> \tag{2.24}$$

$$\frac{M}{N_m \mu_m^{atom}} = \frac{M}{M_s} = B_J[H + \lambda_w M] \tag{2.25}$$

Under appropriate conditions, this leads to solutions for which there is a non-zero magnetization (spontaneous magnetization) even in the absence of an applied field.

For $T > T_c$, the ferromagnetic T_c the only solution to equation (2.25) is $M = 0$, i.e., no spontaneous magnetization and thus paramagnetic response. For $T < T_c$, we

obtain solutions with a non-zero, spontaneous magnetization, the defining feature of a ferromagnet.

Ferromagnetic exchange interactions set the scale for T_c in ferromagnetic alloys. Interatomic exchange couplings can be calculated from first principles by considering the energy change associated with rotation of individual spins in the host material. These exchange interactions can be used within a mean field theory to estimate the T_c. An empirical description of the variations of the exchange energy with inter-atomic spacing called the Bethe-Slater curve is instructive in describing the effect of alloying on ferromagnetic T_c. The interplay between electron-electron Coulomb interactions and the constraints of the Pauli's exclusion principle determine the sign of the exchange interaction.

In transition metal solids a measure of the overlap between nearest neighbor d-orbital is given by the ratio of the atomic to the 3d ionic (or nearest neighbor) radius. In mean field theory the T_c can be related to the exchange energy as follows:

$$T_C = \frac{2S(S+1)}{3K_B}\sum_{ij} T_{ij} \quad , \tag{2.26}$$

where S is the total spin angular momentum, K_B is the Boatman's constant and T_{ij} is the exchange interaction between atoms at the position r_i and r_j.

In first case, a unique constant exchange interaction between the magnetic atoms is assumed and the amorphous nature of the alloy is taken into account by calculating a random distribution of the local anisotropy field [2.34]. In the second approach is treating this problem of distribution of exchange integrals assumed in order to reflect the structural fluctuations in the amorphous alloy. Both approaches predict that M vs. T curve will flat below that for the crystalline counterpart.

EXPERIMENTAL DETAILS

3.1 Methods used for preparation of Nanocrystalline Alloy

There are various techniques in use to produce a metallic alloy in an amorphous state whose the atomic arrangement has no long range periodicity. The methods are generally classified into two groups:

(i) The atomic deposition methods.

(ii) The fast cooling of the melt.

As we know, controlled crystallization from the amorphous state is the only method which presently available to synthesize nanocrystalline alloys with superior soft magnetic properties. In this thesis work amorphous ribbons have been prepared by fast cooling of the melt.

3.1.1 The Fast Cooling of the Melt

The molten alloy must be cooled through the temperature range from the melting temperature (T_m) to the glass transition temperature (T_g) very fast allowing no time for crystallization. The factors controlling T_g and crystallization are both structural and kinetic. Atomic arrangement, bonding and atomic size effects are related in the structural factors. The structural factors as discussed by D. Turnbull [3.1] are the nucleation, crystal growth rate and diffusion rate compared to the cooling rate. The pioneering work of P. Duwez, *et. al.* [3.2], number of devices have been reported for obtaining the necessary high quenching rates and producing continuous filaments. The methods using the principle of fast cooling of melt techniques are:

(i) The gun techniques

(ii) Single roller rapid quenching techniques

(iii) Double roller rapid quenching techniques

(iv) Centrifuge and rotary splat quencher techniques

(v) Torsion catapult techniques

(vi) Plasma-jet spray techniques

(vii) Filamentary casting techniques

(viii) Melt extraction techniques

(ix) Free-jet spinning techniques

(x) The melt spinning techniques

Although the different methods used in preparing amorphous metallic ribbons are mentioned here, only the single roller rapid quenching technique, which is widely used to prepare the amorphous ribbons.

3.1.2 Master Alloy Preparation

Amorphous ribbons with the composition $Fe_{72.5}Ag_2Nb_3Si_{13.5}B_9$ was prepared in an arc furnace on a water-cooled copper hearth under an atmosphere of pure Ar. Their purity and origin of the constituent elements were Fe (99.9%), Ag (99.9%), Nb (99.9%), Si (99.9%) and B (99.9%) as obtained from Johnson Mathey (Alfa Aesar Inc.). The required amounts of the constituent elements were taken from pure metal bars or flakes, weighed carefully with a sensitive electronic balance and placed on the copper hearth inside the arc furnace. Constituent elements in the correct proportions were mixed and melted in the arc-melting furnace under vacuum of 10^{-6} mbar pressure. In order to homogenize perfectly, the alloys were melted three times.

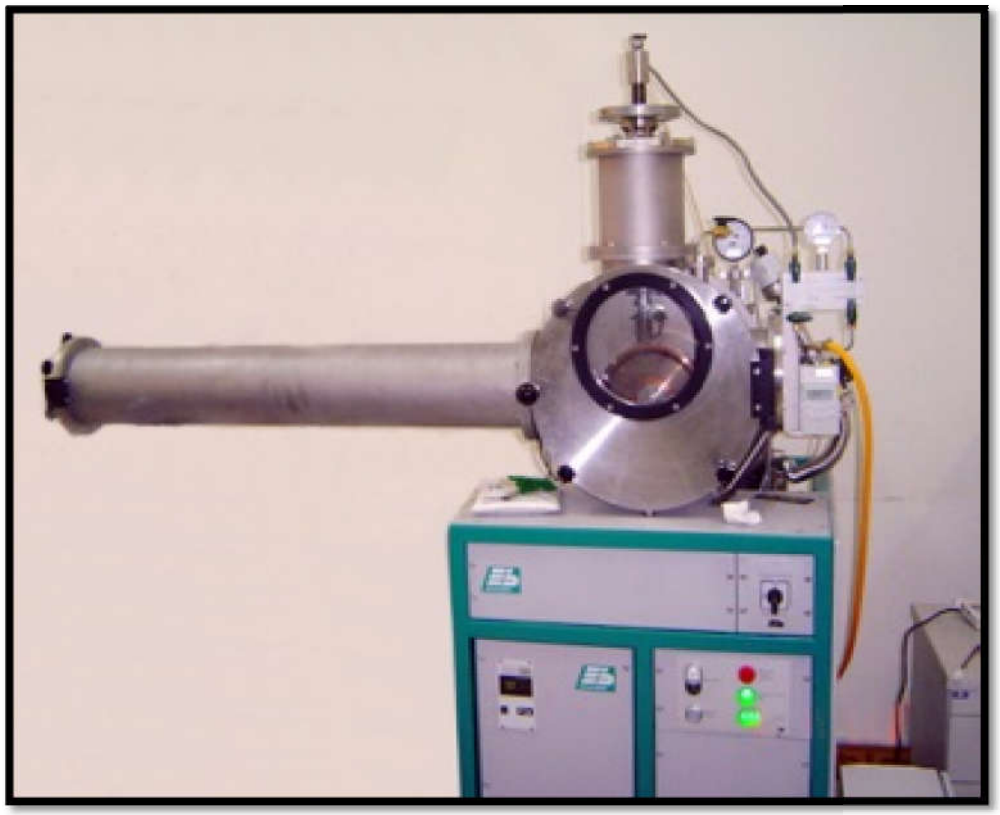

Figure 3.1 : Vacuum Arc Melting Machine

Before melting, the furnace chamber was evacuated (10^{-4} torr),and flashed with Ar gas. The process was repeated several times to get rid of residual air and finally the furnace chamber were kept in an Ar atmosphere. The mother alloys are formed in the form of buttons in a furnace by sudden cooling and is then cut into small pieces and is introduced in the quartz tube. The quartz tube is connected from the top by rubber 'O' rings and metal rings to a Ar cylinder through a valve and a pressure gauge.

A substantial amount of pure Titanium getter, placed inside of the chamber on the side of the copper hearth was melted first in order to observe any oxygen present in the furnace chamber. The constituent elements were then melted in the shape of buttons. The arc melting facilities used to prepare the sample are installed at the Centre for Materials Science, National University of Hanoi, Vietnam. The arc furnace used in the preparation of master alloy is shown in Figure 3.1

3.1.3 Preparation of Ribbon by Melt Spinning Technique

Amorphous alloys in the form of ribbons have been prepared by melt-spinning technique in air. Melting of material is performed by a high frequency generator with water-cooled induction coil. Melt spinning is a widely used production method for rapidly solidifying materials as well as preparing amorphous metallic ribbon [3.3 - 3.4]. In order to prepare amorphous of $Fe_{72.5}Ag_2Nb_3Si_{13.5}B_9$ alloy, the melt spinning facilities was used at the Centre for Materials Science, National University of Hanoi, Vietnam.

The arc melted master alloy was crashed into small pieces and put inside the quartz tube crucible for re-melting by induction furnace using a medium frequency generator with maximum power of 25kW at a nominal frequency of 10kHz. Figure 3.2 shows schematic diagram and Figure 3.3 shows the pictorial view of the Melt-Spinning Machine. The Quartz crucible has in its bottom part, a rectangular nozzle tip of 8 mm length and 0.7 mm width. The ingots were then poured into quartz tube having an orifice diameter of 1mm. Quartz tube was placed inside an induction coil associated with machine. A steel casing covers whole assembly of single roller melt-spin machine. In the beginning the chamber inside the casing was flashed by Ar gas three times. The chamber was then filled with Ar gas The alloys ingots were then melted by induction melting. Appropriate temperature of the melt was assumed from

the color by eye estimation. When color of the melt was appropriate amorphous were obtained.

The position of the nozzle tip can be adjusted with respect to cooper wheel surface, so that the molten alloy was perpendicularly ejected onto the wheel surface from a distance of about 0.3 mm. The small piece of the master alloy samples were inductively remelted inside the quartz tube crucible followed by ejecting the molten metal with an over pressure of 250 mbar of 99.9% pure Ar supplied from an external reservoir through a nozzle onto a rotating copper wheel with surface velocity of 30 m/sec. The temperature was monitored by an external pyrometer from the upper surface of the molten alloy through a quartz window.

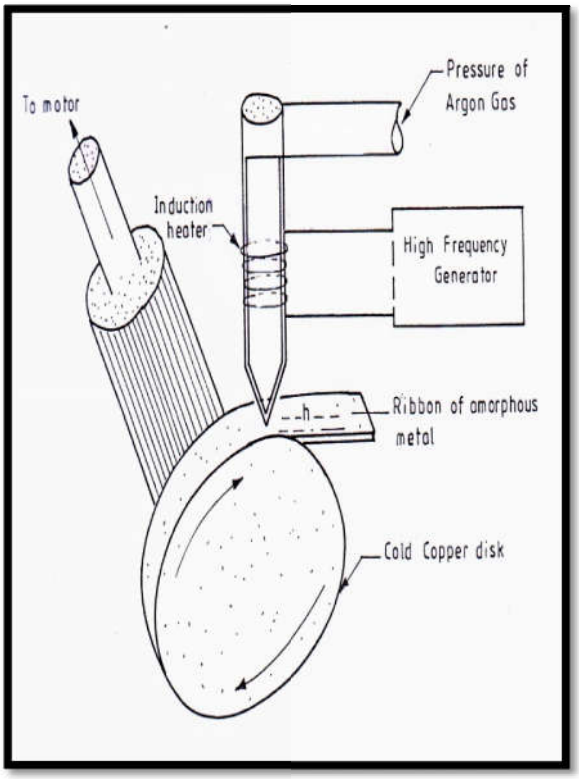

Figure 3.2 : Schematic diagram Figure Figure 3.3 : Melt-Spinning Machine

The metal alloys were ejected at a temperature of about 150 to 250 K above the melting point of the alloy. The resulting ribbon samples had thickness of about 20-25 μm and width ~6 mm. Processing parameters such as the thermal conductivity of the rotating quench wheel, wheel speed, ejection pressure, thermal history of the melt before ejection, distance between nozzle of quartz tube and rotating wheel, as well as processing atmosphere have influenced on the microstructure and properties of melt-

spun ribbons. The lower pressure of 250 mbar as mentioned above stabilizes the turbulence between melt pull and rotating copper wheel enhancing the heat transfer resulting in a more uniform quenching. As a result, a more uniform ribbon microstructure can be obtained at relatively low wheel speed. With increasing wheel speeds for a given ejection rate, the increasing extraction rate results in thinner ribbons.

3.1.4 Important Factors to Control the Thickness of Ribbons

(i) Rotating speed

- Angular velocity ω = 2000rev/min
- Surface velocity V = 20 m/s to 30 m/s

(ii) Gap between nozzle and rotating copper drum (h) = 200 to 30 μm

(iii) Oscillations of the rotating copper drum both static and dynamic has maximum displacement 1.5 to 5 μm

(iv) Pressure = 0.2 to 3.0 bar at argon atmosphere

(v) Temperature of molten metals $T_m \approx 1500^0$C;the temperature did not exceed 1800^0 C otherwise quartz tube would be melted.

(vi) A steady flow of the molten metals on the surface of the rotating drum needs to be ensured.

3.1.5 Confirmation of Amorphousity Ribbons

The amorphous state of the four ribbons has been confirmed by X-ray diffraction using BUKER D8 ADVANCE XRD system located at Bangladesh Council of Scientific and Industrial Research (BCSIR).

From the X-ray diffraction pattern of the sample in Fig. 3.4, there have no peaks observed within the scanning range. Although there is a small hump shown in the diffraction pattern around $2\theta = 45^o$; but it cannot be regarded due to the crystalline effects. So from all the pattern of X-ray diffraction is confirmed that the samples are in pure amorphous state.

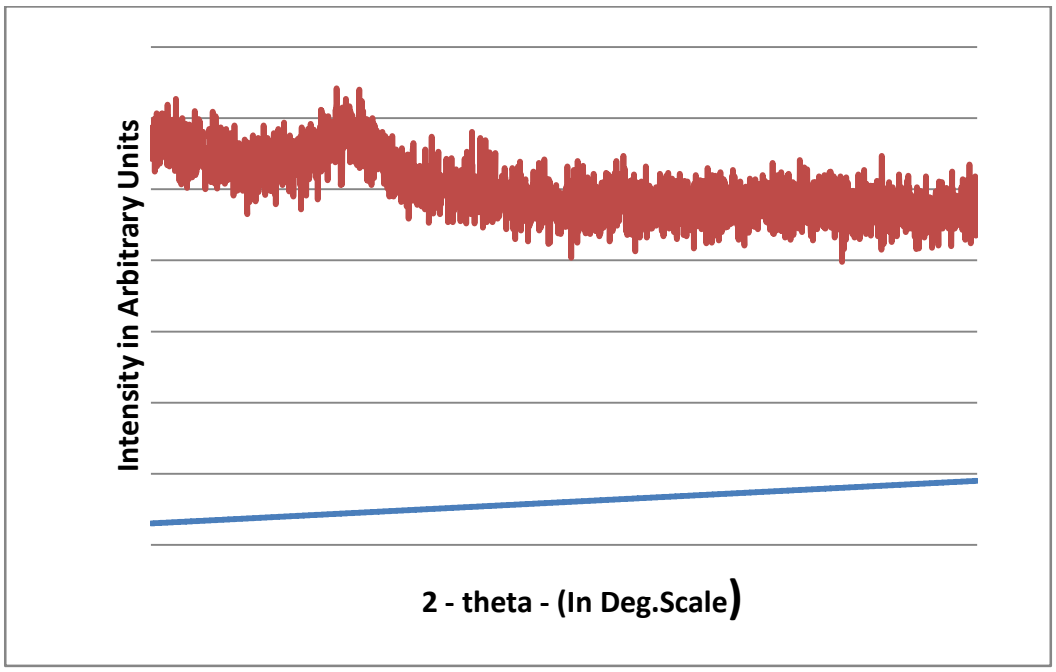

Figure 3.4 : X-ray diffraction of as-cast nanocrystalline amorphous ribbons with Composition $Fe_{72.5}Ag_2Nb_3Si_{13.5}B_9$

3.2 The Principle of Differential Thermal Analysis

Thermal analysis comprises of a group if techniques in which a physical property of a substance is measured as a function of temperature, while the substance is subjected to a controlled temperature program. The Differential Thermal Analysis (DTA) technique was first suggest by Le Chatelier [3.5] in 1887 and was applied to the study of clays and ceramics. DTA involves heating or cooling a test sample and inert reference under identical conditions, while recording any temperature difference between the sample and reference. DTA is the process of accurately measuring the difference in temperature between a thermocouple embedded in a sample and a thermocouple in a standard inert material such as aluminum oxide, while both are being heated at a uniform rate. These differences of temperature arise due to phase transition or chemical reactions in the sample involving the evolution of heat or absorption of heat due to exothermic reaction or endothermic reaction measured. The exothermic and endothermic reactions are generally shown data in the DTA trace as positive and negative deviations respectively from a baseline. Then this differential temperature is plotted against time, or against temperature. When a sample and reference substance are heated or cooled at a constant rate under identical

environment, their temperature differences are measured as a function of time or temperature as shown by the curve in Figure3.5 (a).

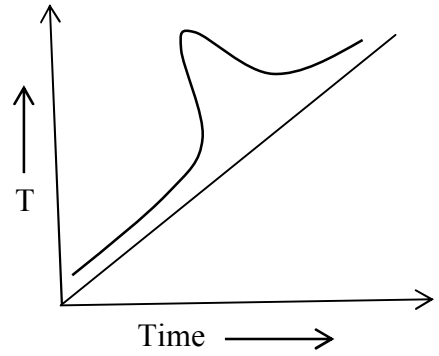

Figure 3.5(a) : Heating curve of sample and reference substance

The temperature of the reference substance, which is thermally inactive, rises uniformly when heated, while the temperature of the sample under study changes anomalously when there is physical or a chemical change of the active specimen at a particular temperature. When there is an exothermic reaction there is a peak in the temperature versus time curve, heat supplied from outside is consumed by the reaction. And when the reaction is over, the sample temperature gradually catch up the temperature of the inactive specimen. The temperature difference ΔT is defined, amplified and recorded by a peak as shown in Figure 3.5 (b).

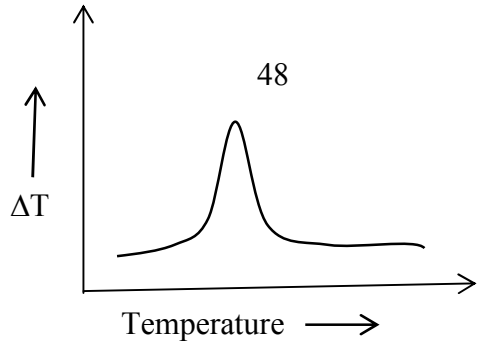

Figure 3.5(b) : DTA Curve

For any endothermic reaction or change the active specimen absorbs heat which is reflected in the corresponding the trough in temperature versus time curve. Changes in the sample, which leads to the absorption or evolution of heat, can be detected relative to the inert reference. Differential temperatures can also arise between two inert samples when their response to the applied heat treatment is not identical. DTA can therefore be used to study thermal properties and phase changes which do not lead to a change in enthalpy.

Changes in the sample, either exothermic or endothermic, can be detected relative to the inert reference. Thus, a DTA curve provides data on the transformations that have occurred, such as glass transitions, crystallization, melting and sublimation. The baseline of the DTA curve showed then exhibit discontinuities at the transition temperatures and the slope of the curve at any point will depend on the microstructural constitution at that temperature. The area under a DTA peak can be related to the enthalpy change and is not affected by the heat capacity of the sample. DTA may be defined formally as a technique for recording the difference in temperature between a substance and a reference material against either time or temperature as the two specimens are subjected to identical temperature regimes in an environment either heated or cooled at a controlled rate.

3.2.1 Apparatus

The DTA is a technique to study the structural change occurring both in solid and liquid materials under heat treatment. These changes may be due to dehydration, transition from one crystalline variety to another, destruction of crystalline lattice, oxidation, decomposition etc. The key features of a DTA kit are as shown in Figure 3.6 sample holder comprising thermocouples, sample containers and a ceramic or metallic block, a furnace, temperature programmer, recording system. The essential requirements of the furnace are that it should provide a stable and sufficiently large hot-zone and must be able to respond rapidly to commands from the temperature programmer. A temperature programmer is essential in order to obtain constant heating rates. The recording system must have a low inertia to faithfully reproduce variations in the experimental set-up.

The sample holder assembly consists of a thermocouple each for the sample and reference, surrounded by a block to ensure an even heat distribution. The sample is contained in a small crucible designed with an indentation on the base to ensure a snug fit over the thermocouple bead. The crucible may be made of materials such as Pyrex, Silica, Nickel or Platinum, depending on the temperature and nature of the tests involved. The thermocouples should not be placed in direct contact with the sample to avoid contamination and degradation, although sensitivity may be compromised. Metallic blocks are less prone to base-line drift when compared with ceramics which contain porosity. On the other hand, their high thermal conductivity leads to smaller DTA peaks.

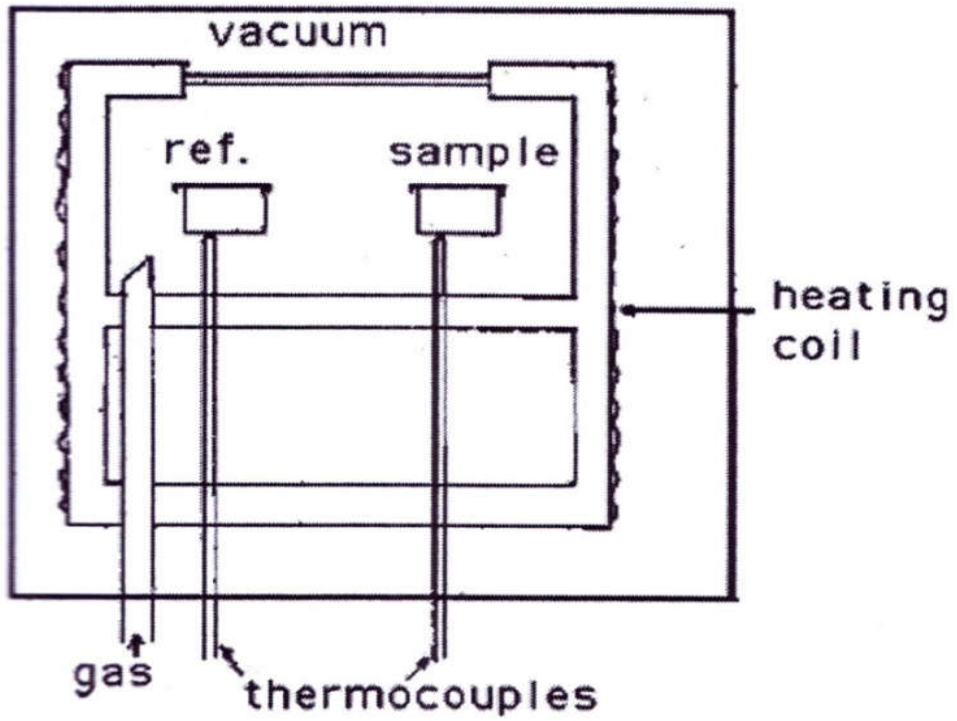

Figure 3.6 : Schematic illustration of a DTA cell

The sample assembly is isolated against electrical interference from the furnace wiring with an earthed sheath, often made of platinum-coated ceramic material. The sheath can also be used to contain the sample region within a controlled atmosphere or a vacuum. The specimen holder is placed in the cavity of the heating block which is operated in the center of the cylindrical refractory tube of an electrical furnace. This supplies is a uniform heating rate. The furnace is peaked with calcined china clay. The input of current into the furnace is secured through the secondary of a Variac transformer, which controls the currents.

Fine Chromelalumel wires (28 gauges) are used for thermocouples. A cold junction is used for thermocouple leads and the emf. is recorded almost continuously, while the temperature of the inert material is measured at 3 minute intervals. It is essential to use perfectly dry materials, as otherwise errors will be introduced in the analysis. Approximately 0.1 gm anhydrous alumina is used in the reference cup and the sample weight varies over a range 0.05 to 0.125 gm; depending on their density. One thermocouple is placed in an inert material such as Al_2O_3 while the other is placed in a sample of the material under study. As the temperature is increased, there will be a brief deflection of the voltmeter if the sample is undergoing a phase

transition. This occurs because the input of heat will raise the temperature of the inert substance, but be incorporated a latent heat in the material changing phase. A heating rate of 10^{o}C to 60^{o}C per minute of the furnace is conveniently chosen and this gives satisfactory results in most case. A block diagram of DTA as shown in Figure 3.7

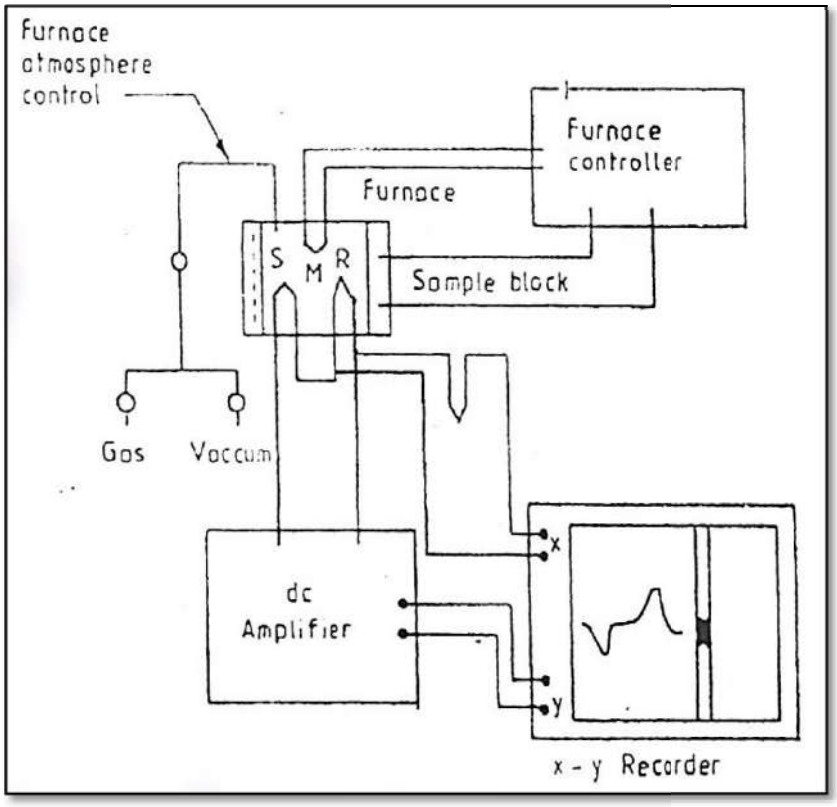

Figure 3.7 : Block diagram of a DTA equipment, (S) sample thermocouple, (R) Reference thermocouple, (M) Monitor thermocouple

During experiments a temperature problems are encountered in transferring heat uniformly away from the specimen. These may be mitigated by using thermocouples in the form of flat discs to ensure optimum thermal contact with the new flat-bottomed sample container, made of aluminum or platinum foil. To ensure reproducibility, it is then necessary to ensure that the thermocouple and container are consistently located with respect to each other.

3.3 Experimental Factors

It is necessary in care to selecting the experimental parameters. For example, the effects of specimen environment, composition, size and surface to volume ratio all affect powder decomposition reactions, whereas these particular variables may not

affect solid state phase changes. Experiments are frequently performed on powders so the resulting data may not be representative of bulk samples, where transformations may be controlled by the build-up of strain energy. The packing state of any powder sample becomes important in decomposition reactions and can lead to large variations between apparently identical samples.

In some circumstances, the rate of heat evolution may be high enough to saturate the response capability of the measuring system; it is better than to dilute the test sample with inert material. For the measurement of phase transformation temperatures, it is advisable to ensure that the peak temperature does not vary with sample size. The shape of a DTA peak does depend on sample weight and the heating rate used. The influence of heating rate on the peak shape and disposition can be used to advantage in the study of decomposition reactions, but for kinetic analysis it is important to minimize thermal gradients by reducing specimen size or heating rate.

3.3.1 Interpretation and Presentation of DTA

There are difficult with the measurement of transition temperatures using DTA curves. The onset of the DTA peak in principle gives the start-temperature, but there may be temperature lags depending on the location of the thermocouple with respect to the reference and test samples or the DTA block. It is wise to calibrate the apparatus with materials of precisely known melting points. The peak area (A), which is related to enthalpy changes in the test sample, is that enclosed between the peak and the interpolated baseline. When the differential thermocouples are in thermal, but not in physical contact with the test and reference materials, it can be shown that A is given by,

$$A = \frac{mq}{gk} \tag{3.1}$$

where m is the sample mass, q is the enthalpy change per unit mass, g is a measured shape factor and k is the thermal conductivity of sample.

With porous, compacted or heaped samples, the gas filling the pores can alter the thermal conductivity of the atmosphere surrounding the DTA container and lead to large errors in the peak area. The situation is made worse when gases are evolved from the sample, making the thermal conductivity of the DTA-cell environment different from that used in calibration experiments. The DTA apparatus is calibrated for enthalpy by measuring peak areas on standard samples over specified temperature

ranges. The calibration should be based upon at least two different samples, conducting both heating and cooling experiments.

Figure 3.8 : TA7000 Series Simultaneous Thermogravimetric Analyzer

In the present work, HITACHI Instruments TA7000 Series Simultaneous Thermogravimetric Analyzer TG/DTA/DSC which is situated at Kulna University of Engineering & Technology (KUET) has been used for thermal analysis shows in Figure 3.8. The Thermo gravimetric/Differential Thermal Analyzer (TG/DTA) combine the flexibility of DTA with the proven capabilities of the TG measurement technology, providing property information for a verity of samples. Thus simultaneous TG/DTA/DSC System can be used for such application as oxidation, heat resistance, and the amount of water, compositional analysis and measurement of ash contents in a sample. This system is also used to cover such need as reaction rate and accelerated degrading tests.

The thermal analysis runs generally for 1 to 1.5 hrs. Thermal analysis curves are obtained by plotting heating temperature and the difference between the temperature of the test and reference substances. From these plots the reaction

temperature could be determined. Under standard conditions of the experiment; characteristic curves for the composition of $Fe_{72.5}Ag_2Nb_3Si_{13.5}B_9$ nanocrystalline amorphous ribbons. T_{x_1} and T_{x_2} points are indicating the sharp exothermic peaks.

All experiments are run at atmospheric pressure in continuous flow of purified inert gas Nitrogen. Gases are normally purged into the furnace chamber at the lower end through a purification train in which oxygen and water are removed by heated copper wool and exhausted from the top into a condensate trap for collecting the condensable volatile products.

A.The Features are:

(i) The TG/DTA can operate in either DSC or DTA mode. In DSC mode it displays heat flow signal.

(ii) The horizontal differential balance provides high sensitivity and accuracy.

(iii) Gas control unit automatically control the environment of the furnace between measurements.

(iv) Auto sampler with 30 samples positions provides laboratory automation and increase productivity.

(v) Through the utilization of an automatic cooling unit, the instrument is now automatically cooled to a set temperature after measurements, which raises the effectiveness of measurements.

B. Specification:

Temperature Range : Room temperature to 1500°C
(normally around 1300°C)

Balance Method : Horizontal differential type

Maximal sample weight : 200mg;

Program rate : 0.01 to 100°C/min

Automatic Cooling unit : Force Air Cooling

Gas flow rate : 0 to 1000ml/min

Cooling rate : less than 15 min from 1000 to 50°C

Atmosphere : Air, Inert gas, Vacuum (10-2 Torr)

Sample pan material : Platinum, Alumina and Aluminum.

TG measurement Range/Sensitivity: 200 mg /0.2µg

DTA measurement / Sensitivity: +1000µV/ 0.06µV

3.3.2 Annealing

Annealing in metallurgy and materials science, is heat treatment wherein a material is altered, causing changes in its properties such as strength and hardness. It is a process that produces conditions by heating to above the critical temperature, maintaining a suitable temperature, and then cooling. Annealing is used to induce ductility, soften material, relieve internal stresses, refine the structure by making it homogeneous, and improve cold working properties.

In the cases of copper, steel, silver and brass, this process is performed by substantially heating the material (generally until glowing) for a while and allowing it to cool. Unlike ferrous metals, which must be cooled slowly to anneal, copper, silver and brass can be cooled slowly in air or quickly by quenching in water. In this fashion the metal is softened and prepared for future work such as shaping, stamping, or forming.

Annealing occurs by the diffusion of atoms within a solid material, so that the material progresses towards its equilibrium state. Heat is needed to increasing the rate of diffusion by providing the energy needed to break bonds. The movement of atoms has the effect of redistributing and destroying the dislocations in metals and (to a lesser extent) in ceramics. This alternation in dislocations allows metals to deform more easily, so increases their ductility.

3.3.3 Stages

There are three stages in the annealing process, with the first being the recovery phase, which results in softening of the metal through removal of crystal defects (the primary type of which is the linear defect called a dislocation) and the internal stresses which they cause. Recovery phase covers all annealing phenomena that occur before the appearance of new strain-free grains. The second phase is recrystallization, where new strain-free grains nucleate and grow to replace those deformed by internal stresses. If annealing is allowed to continue once recrystallization has been completed, grain growth will occur, in which the microstructure starts to coarsen and may cause the metal to have less than satisfactory mechanical properties.

3.3.4 Setup and Equipment

Typically, large ovens are used for the annealing process. The inside of the oven is large enough to place the work piece in a position to receive maximum exposure to the circulating heated air. For high volume process annealing, gas fired conveyor furnaces are often used. For large work piece or high quantity parts, car-bottom furnaces will be used in order to move the parts in and out with ease. Once the annealing process has been successfully completed, the work pieces are sometimes left in the oven in order for the parts to have a controlled cooling process. While some work pieces are left in the oven to cool in a controlled fashion, other materials and alloys are removed from the oven. After being removed from the oven, the work pieces are often quickly cooled off in a process known as quench hardening. Some typical methods of quench hardening materials involve the use of media such as air, water, oil or salt. Quench hardening is generally applicable for some ferrous alloys, but not copper alloys.

3.4 Thermal Treatment of the Nanocrystalline Amorphous Ribbon

With a view to study nanocrystallization behavior by XRD and magnetic properties upon evaluation of nanocrystalline phase on amorphous matrix, thermal treatment, i.e. annealing is required to perform.

Figure 3.9 : MTI - GSL-1600x40 Tube Furnaces

For XRD, as prepared amorphous ribbon were cut into small pieces of about 2cm lengths for annealing treatment. MTI Corporation built GSL-1600x40 tube furnace used for this purpose shown in Figure 3.9. The samples were put into the tube and filled up with Nitrogen gas before the tube furnace heated to a predefined temperature and kept for the time (2 hrs) required completing the annealing. In this way all the isothermal annealing as a function of time were performed.

3.5 Powder/ Polycrystalline Diffraction

About 90% of all solid materials can be described as crystalline. When X-ray interacts with a crystalline substance (phase) one get a diffraction pattern. The X-ray diffraction pattern of a pure substance is, therefore, like a fingerprint of the substance. The powder diffraction method is thus ideally suited for characterization and identification of polycrystalline phases. Today about 50000 inorganic and 25000 organic single components, crystalline phase and diffraction patterns have been collected and stored on magnetic or optical media as standers. The main use of powder diffraction is to identify components in a sample by a search match procedure. Furthermore, the areas under the peak are related to the amount of each phase present in the sample.

3.5.1 Theoretical Considerations of X-ray Diffraction (XRD)

The German Physicist Wilhelm Roentgen discovered X-rays in 1895. X-rays are electromagnetic waves of short wavelengths in the range of 10^{-2} to 10^{2}Å. Unlike ordinary light, these rays are invisible, but they travel in straight lines and affect photographic film in the same way as light. On the other hand, they were much more penetrating than light and could easily pass through the human body, wood, quite thick pieces of metal and other “opaque” objects.

The XRD provides substantial of information on the crystal structure. XRD is one of the oldest and effective tools for the determination of the atomic arrangement in a crystal. The wavelength (1Å) of an X-ray is the same order of magnitude as the lattice constant of crystals and it is this which makes X-rays so useful in structural analysis of crystal. Whenever X-rays are incident on a crystal surface, they are reflected from it. The reflection abides by the Bragg’s Law as given below

$$2d\sin\theta = n\lambda \qquad (3.2)$$

Where d is the distance between crystal plane, θ is the incident angle, λ is the wavelength of the X-ray and n is a positive integer. Bragg's Law also suggested that the diffraction is only possible when $\lambda < 2d$.

X-ray diffractograms of all the samples were recorded using monochromatic Cu-K_α radiation (λ = 1.54053 Å) to ensure the formation of single-phase nature of the product. XRD patterns information are: scanning speed 2°, chart speed 20 mm, starting from 20° and ending at 90°. Peak intensities are recorded corresponding to their 2θ values. The inter planner distance - d was calculated from these 2θ values of the diffraction peaks using the Bragg's Law (In Figure 3.10).

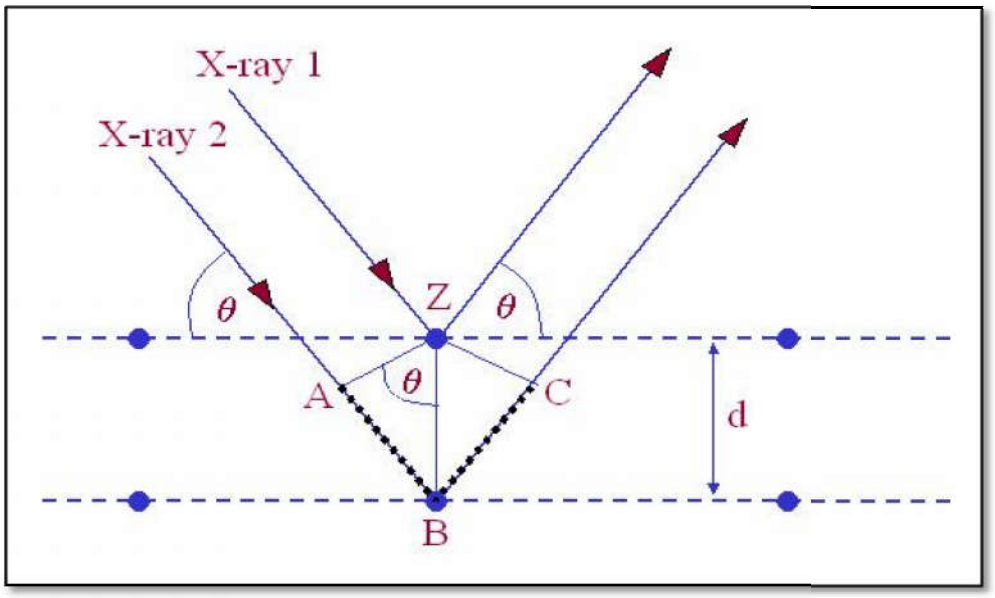

Figure 3.10 : Bragg's diffraction pattern

Therefore the two possible values where we can have reflections are determined by the unit cell dimensions. However, the intensities of the reflection are determined by the distribution of the electrons in the unit cell. The highest electron density is found around atoms. Therefore, the intensities depend on what kind of atoms we have and where in the unit cell they are located. Planes going through areas with high electron density will reflect strongly, planes with low electron density will give weak intensities.

3.5.2 X-ray Powder Method

Powder method is perhaps the most widely used X-ray diffraction technique for characterizing materials. The term 'powder' really means that the crystalline domains are randomly oriented in the sample. Therefore, when the 2-D diffraction pattern is recorded, it shows concentric rings of scattering peaks corresponding to the various d spacing in the crystal lattice. The positions and the intensities of the peaks are used for identifying the underlying structure (or phase) of the material. Powder diffraction data can be collected using either transmission or reflection geometry, as shown in Figure 3.11 below.

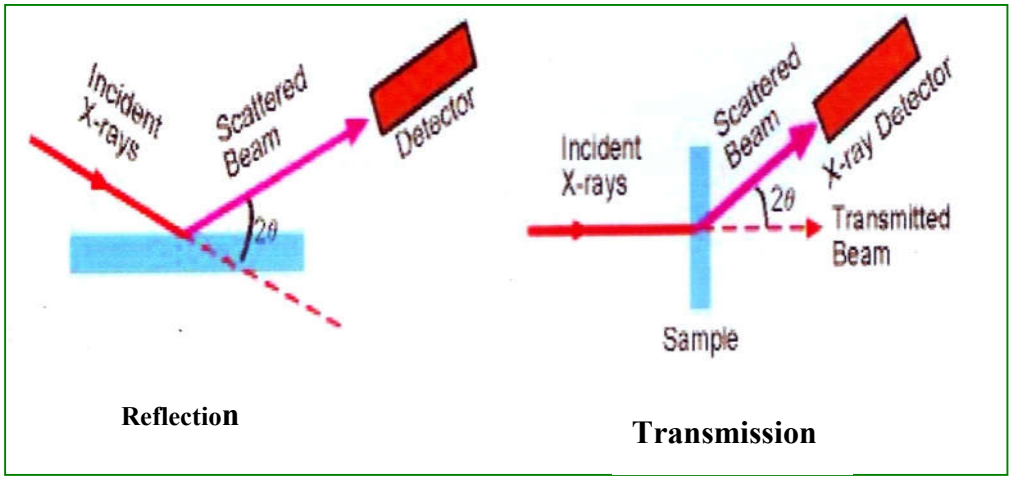

Figure 3.11 : Reflection and Transmission geometry of powder diffraction

Because the particles in the powder sample are randomly oriented, these two methods will yield the same data. Powder diffraction data are measured using Bruker AXS D8 Advance diffractometer, which measures data in reflection mode and is used mostly with solid samples, or the custom built 4-circle diffractometer, which operates in transmission mode and is more suitable for liquid phase samples.

3.5.3 Experimental Technique for X-ray Diffractometer

X-ray diffraction (XRD) is a versatile non-destructive analytical technique for identification and quantitative determination of various crystalline phases of powdered or solid samples of any compound. For each set of composition, ribbons are cut into several pieces; each of length 20 mm. Heat treatment was performed on the amorphous ribbons using a tube furnace which filled by Nitrogen gas. After the heat treatment, samples were removed from the furnace tube carefully and kept separately for XRD experiment.

For XRD experiment each sample was set on a glass slides and fixed the sample by putting adhesive tape at the two ends of the sample. After the pattern is obtained the value of 2θ is calculated for each diffraction line; set of 2θ values is the raw data for the determination of the lattice parameters of the unit cell. Figure 3.12: Shows the block diagram of Bruker AXS D8 Advance X-ray diffractometer. The Bucker AXS D8 Advance X-ray diffractometer was used for the lattice parameter determination in the PP&PDC, Materials Science Division, Bangladesh Council of Scientific and Industrial Research (BCSIR), Dhaka. Figure 3.13 shows the inside view of the Bucker AXS D8 Advance XRD system. The Bruker AXS D8 Advance diffraction system utilizes a modular system approach to provide performance for application ranging from routine characterization to in-depth research investigation.

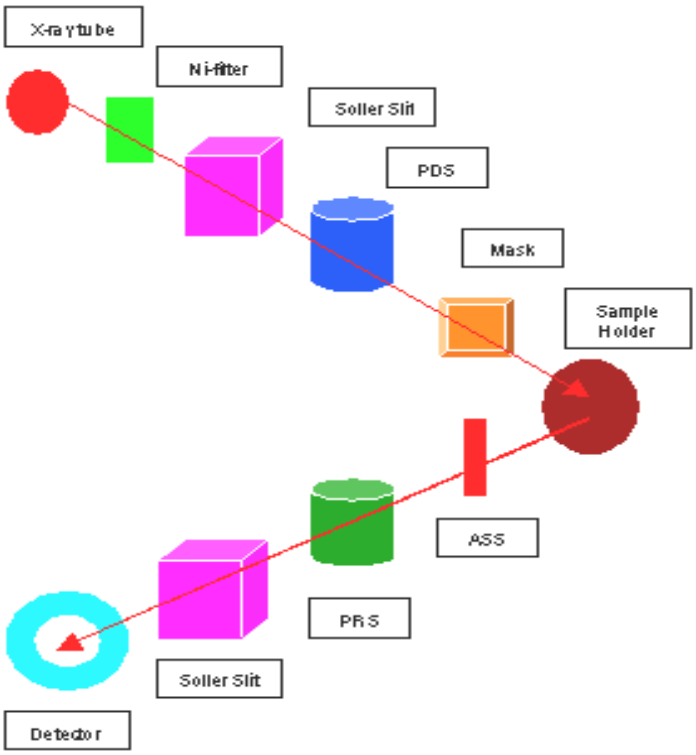

Figure 3.12 : Block diagram of the Bruker AXS D8 Advance XRD system

The powder diffraction technique was used with a primary beam power of 40 kV and 40 mA for Cu radiation. A nickel filter was used to reduce Cu-K_α radiation and finally Cu-K_α radiation was only used as the primary beam. A (θ- 2θ) scan was taken from 30^o to 90^o to get possible fundamental peaks of the sample with the sampling pitch of 0.02^o and time for each step data collection was 1.0 sec. Both the programmable divergence and receiving slits were used to control the irradiated beam

area and output intensity from the sample respectively. During XRD analysis, X-ray beams are reflected off a specific wavelength, for any given d-spacing (distance between adjacent atomic planes) there are only specific angles at which the exiting rays will be 'in phase' and therefore, will be picked up by the detector producing a peak on the 'diffractogram'. Just like a 'fingerprint', every mineral has it own distinct set of diffraction peak that can be used to identify it.

An anti-scatter slit was used just after the sample holder to reduce air scattering. Two solar slits were used just after the tube and in front of the detector to get parallel beam only. All the data of the samples were stored in the computer memory and later analyzed that using computer software "DIFFRAC^{plus}".

Figure 3.13 : Bruker AXS D8 Advance

The Bruker AXS D8 ADVANCE has the ability to perform a full range of applications, from qualitative and quantitative phase identification, under ambient or non-ambient conditions, to crystal structure solution from powder samples, crystallite size determination, micro strain analysis, residual stress analysis, and preferred orientation.

Bruker AXS D8 Advance SPECIFICATIONS	
X-RAY SOURCE	2.2kW Cu and Co, Running condition (40kV, 40mA), Power stability is better than 0.01%
DETECTORS	Point detector, Vantec-1 detector
OPTICS	Gobel Mirror
GONIOMETER	High precision microprocessor controlled, two circle goniometer with independent stepper motors and optical encoders; Smallest angular step 0.0001°; Reproducibility +/- 0.0001°
SAMPLE STAGE	Centric ¼-Circle Eulerian Cradle.Motorized Chi (tilt) and Phi (rotation) rotations and X-Y-Z translations. The cradle accommodates bulky specimens, powders, thin-films, and wafers up to 80 x 50 x 20 mm and weighing up to 1 kg
ATTACHEMENTS	High Temperature MRI stage (RT-1400C), Thin Film Reflectometry, sample spinner, video camera, sample plate with 9-sample holders
SOFTWARE	LEPTOZ, TOPAZ, ICCD

Attributes	
Depth	1135 mm
Height	1868 mm
Width	1300 mm
Weight	770 kg
Additional Specifications	Configurations: Vertical goniometer, Theta/2Theta or Theta/Theta geometry Measuring circle diameter: Predefined at 500 mm, 560 mm and 600 mm or any intermediate setting Angular range: 360° Max. usable angular range: –110° < 2Theta 168° Angle positioning: Stepper motors with optical encoders Smallest addressable increment: 0.0001° Instrument alignment: Equal or better than ± 0.01° 2Theta; NIST SRM 1976a always included Maximum angular speed: 20°/s Detectors: Point detectors: Scintillation counter SOL-XE energy dispersive 1-D detectors: LYNXEYE, VÅNTEC-1 All detectors guaranteed without defective/dead strips or areas Cooling water supply: Min. 4 l/min, pressure 4 bar to 7.5 bar, no pressure on outlet side, temperature: 10 °C to 20 °C Power supply: Single phase: 208 to 240 V, Three phases: 120 V, 230 V, 240V; 47 to 63 Hz

3.6 Analysis of XRD data

The XRD data consisting of $\theta_{hkl}$and d_{hkl} values corresponding to the different planes from which the following structural information of the nanocrystalline ribbon sample was evaluated.

(i) Identification of phases

(ii) Lattice parameter determination

(iii) Average grain size determination

(iv) Si- content determination in nanograins

(i) Identification of phases

The most common use of powder (polycrystalline) diffraction is chemical analysis. This can include phase identification (search/match), investigation of high/low temperature phase, solid solutions and determination of unit cell parameter of new materials.

XRD has become a very popular and useful instrument for routine X-ray analysis of nanocrystalline amorphous ribbon samples. In fact the diffractometer technique is often preferred to Debye-Scherrer technique owing to its several inherent merits. The most striking difference between the two methods is in the use of different intensity detection and measuring devices. XRD pattern of as-cast indicates just amorphous pattern of the given composition. The XRD patterns are identified as bcc α-Fe (Si) solid solution, which are developed on the nanocrystalline amorphous ribbon after heat treatment. The peak pattern is observed for all the samples at different heat treatment temperatures indicating the bcc α-Fe (Si) phase, which is developed on amorphous ribbons after heat treatment. Present experiment revels that 450°C is not sufficient temperature to start forming of crystalline nanograins of bcc Fe (Si) on the amorphous ribbon of the studied alloy composition.

(ii) Lattice Parameter Determination

Lattice parameter of crystalline bcc Fe-Si nanograin has been determined for all the two different amorphous compositions at different heat treatment temperatures. Normally, lattice parameter of an alloy composition is determined by the Debye-Scherrer method after extrapolation of the curve. In the present case, only one reflection (110) is prominent in all XRD patterns and we would like to understand how the value of lattice parameter changes with annealing temperature. We have,

therefore, determined the lattice parameter using only that particular reflection using equation $2d\sin\theta = \lambda$ and $a_0 = d\sqrt{2}$, where $\lambda = 1.54178\text{Å}$ for $Cu - K_\alpha$ radiation and a_0 is the determined lattice parameter within an error estimated to be $\pm 0.0001\text{Å}$.

(iii) Grain Size Determination

The main aim (vital point) of the present study is to determine the nanocrystalline grain size for all the heat treated samples of the alloy composition by using Scherrer method. The XRD pattern of (110) reflection for different steps of heat treatment temperature of the alloy composition is used to calculate grain size. Grain size is determined using the following formula,

$$D_g = \frac{0.9\lambda}{\beta\cos\theta} \tag{3.3}$$

Where $\lambda = 1.54178\text{Å}$ for $Cu - K_\alpha$ radiation and β = FWHM (full width at half maximum) of the peak in radian. Considering β in degree we get the following relation

$$D_g = \frac{79.5}{\beta\cos\theta} \tag{3.4}$$

All the values of grain size for every steps of heat treatment temperature of the alloy composition were determined. The FWHM of the peak is large at the early heat treatment temperature and with the increase of heat treatment temperature the value of FWHM becomes smaller which means that the grain size is increasing gradually.

(iv) Si-content in Nanograins

Crystalline nanograins were formed on the amorphous matrix of the ribbon in the process of heat treatment having the composition of Fe-Si. It is, therefore important to determine the concentration of Fe and Si in the nanograin [2.15]. As because the alloy consists of Fe and Si and we have experimentally determined the lattice parameter of the alloy nanograin for the two compositions at different temperatures. It is easy to calculate the Si content in the nanograins from the data of Pearsons who was established the relationship between the lattice parameter as dependent on Si content in Fe-Si alloys covering a wide range of composition [3.6]. From the relationship, we have constructed a simple equation to calculate Si content from lattice parameter. The equation is

$$X = \frac{(a_0 - 2.8812)}{0.0022} \tag{3.5}$$

Where X is at. % Si in the nanograins, a_0 is the determined lattice parameter of nanograins. Si-contents for the nanograins develop during the isothermal annealing at various temperatures have been calculated.

3.7 Magnetization Measurement Techniques

In the present study magnetization has been performed using a Vibrating Sample Magnetometer (VSM).

3.7.1 Vibrating Sample Magnetometer (VSM)

A vibrating sample magnetometer (VSM) operates on Faraday's Law of Induction, which tells us that a changing magnetic field will produce an electric field. This electric field can be measured and can tell us information about the changing magnetic field. A VSM is used to measure the magnetic behavior of magnetic materials. VSM is a versatile and sensitive method of measuring magnetic properties developed by S. Foner [3.7-3.8] and is based on the flux change in a coil when the sample is vibrated near it. The VSM is designed to continuously measure the magnetic properties of materials as a function of temperature and field. In this type of magnetometer, the sample is vibrated up and down in a region surrounded by several pickup coils. The magnetic sample is thus acting as a time-changing magnetic flux, varying inside a particular region of fixed area. From Maxwell's law it is known that a time varying magnetic flux is accompanied by an electric field and the field induces a voltage in pickup coils. This alternating voltage signal is processed by a control unit system, in order to increase the signal to noise ratio. The result is a measure of the magnetization of the sample.

3.7.2 Principle of VSM

The principle of VSM is as follows: when the sample of a magnetic material is placed in a uniform magnetic field, a dipole moment proportional to the product of the sample susceptibility times the applied field is induced in sample. If the sample is made to undergo a sinusoidal motion, an electrical signal is induced in suitably located stationary pick-up coils. This signal which is at the vibrating frequency, is proportional to the magnetic moment, vibration amplitude and vibration frequency. In order to obtain the reading of the moment only, a capacitor is made to generate another signal for comparison which varies in its moment, vibration amplitudes and vibration frequency in the same manner as does the signal from the pick-up coil.

These two signals are applied to the two inputs of a differential amplifier, and because the differential amplifier passes only difference between the two signals, the effects of vibration amplitude and frequency changes are cancelled. Thus only the moment determines the amplitude of the signal at the output of the differential amplifier. This signal is in turns applied to a lock-in amplifier, where it is compared with the reference signal which is at its internal oscillator frequency and is also applied to transducer which oscillation the sample rod. Thus the output of the lock-in amplifier is proportional to the magnetic moment of the sample only avoiding any noise of frequency other that of the signal. The lock-in action yields an accuracy of 0.05% of full scale. The absolute accuracy of this system is better than 2% and reproducibility is better than 1%. Least measureable moment is $\mathbf{5 \times 10^{-4}}$ emu.

Figure 3.14 : Vibrating Sample Magnetometer (VSM)

These measurements were carried out at Materials Science Division, Atomic Energy Center, Dhaka. We use Hirst VSM02 which is an automatic VSM for characterization of soft and hard magnetic materials manufactured by HIRST Magnetic Instruments Ltd. The Hirst VSM system arrangement is shown in the Figure 3.14.

RESULTS AND DISCUSSION

4.0 Results and Discussion

4.1 Differential Thermal Analysis Results

The structure of the beneficial ferromagnetic nanocrystalline phase is composed of α-Fe(Si), which is the product of primary crystallization. The change of composition affects the growth kinetics in a complicated way, which can only be determined experimentally. This phase is determintal for the soft magnetic properties because of its high anisotropy energy. The understanding of the crystallization kinetics of magnetic amorphous alloys is of scientific interest as it represents a phase transformation occuring under extreme conditions far from equilibrium. Crystallization kinetics of magnetic materials is often determined from Differential Scanning Calorimetry (DSC), Differential Thermal Analysis (DTA) and Thermomagnetic Analysis (TMA) [4.1-4.3]. The calorimetric studies of amorphous alloys provide substantial fundamental information concerning the kinetics of the crystallization have been studied calorimetrically by Clements and Cantor [4.4] and both calorimetrically and magnetically by Luborsky [4.5] in a variety of amorphous magnetic alloys. If the amorphous alloy is to be used as a precursor for the production of nanocrystalline FINEMET of composition Fe-Ag-Nb-B-Si then the primary and secondary crystallization temperatures are of importance. The change of composition affects crystallization phases, because the time needed for the constituted atoms to arrange themselves in a long range order depends on their bond energies [4.6].

In the present investigation DTA technique has been used to study the crystalline behavior of nanocrystalline alloy with composition $Fe_{72.5}Ag_2Nb_3Si_{13.5}B_9$. The crystallization process is affected by heating rate as well as by composition. To keep the stability of the nanocrystalline alloy to achieve the expected soft magnetic behavior, both the nucleation and growth rate of nanocrystalline must be controlled. DTA data are then analyzed within frame work of kinetic rate law and activation energy for corresponding crystallization peak extracted. Crystallization have also been studied by a sign X-ray diffraction (XRD). The X-ray diffraction experiment was undergone to identify the revolution of phases with heat treatment.

4.1.1 DTA Results of Nanocrystalline Amorphous Ribbon with Composition $Fe_{72.5}Ag_2Nb_3Si_{13.5}B_9$

DTA traces of as-cast nanocrystalline amorphous ribbon $Fe_{72.5}Ag_2Nb_3Si_{13.5}B_9$ alloy taken in nitrogen atmosphere with the heating rates of 10^oC – 60^oC/minute at the step of 10^oC with continuous heating from room temperature to 800^oC, are presented in Figure 4.1 (a) to Figure 4.1 (f), respectively. In each of the figure, one exothermic peak is distinctly observed which corresponds to crystallization event at temperature T_{x_1}. The soft magnetic ribbon corresponds to close in which primary crystallization (T_{x_1}) of α-Fe(Si) takes place. XRD has been used for the identification of phases and would be discussed later on. Thus, the identification of this temperature, is necessary to understand the appropriate temperature range for heat treatment in order to achieve the nanocrystalline phase and thereby, suitable range of temperature for application of alloy.

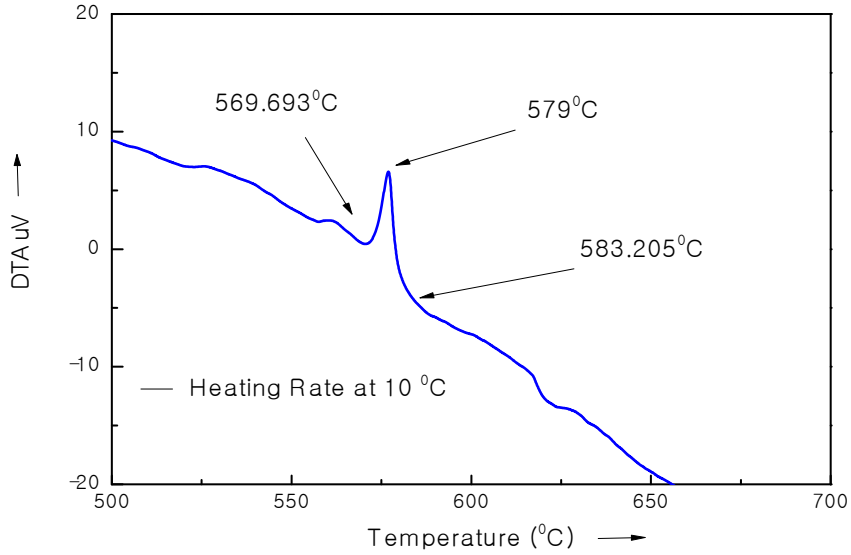

Figure 4.1 (a) : DTA trace of as-cast nanocrystalline amorphous ribbon $Fe_{72.5}Ag_2Nb_3Si_{13.5}B_9$ at the heating rate of 10^oC/min

DTA is a direct and effective way to analyze the kinetics of nanocrystalline materials in respect of phase transition. The change of composition affects atomic ordering through nucleation and growth of crystallites. The transition from amorphous to crystalline state is an exothermic process. It means the peak arise due to release of heat energy at particular temperature. At that temperature, atoms are arranged in a

crystalline periodic order, i.e. in a long range order atomic order by consuming heat energy supplied through the process.

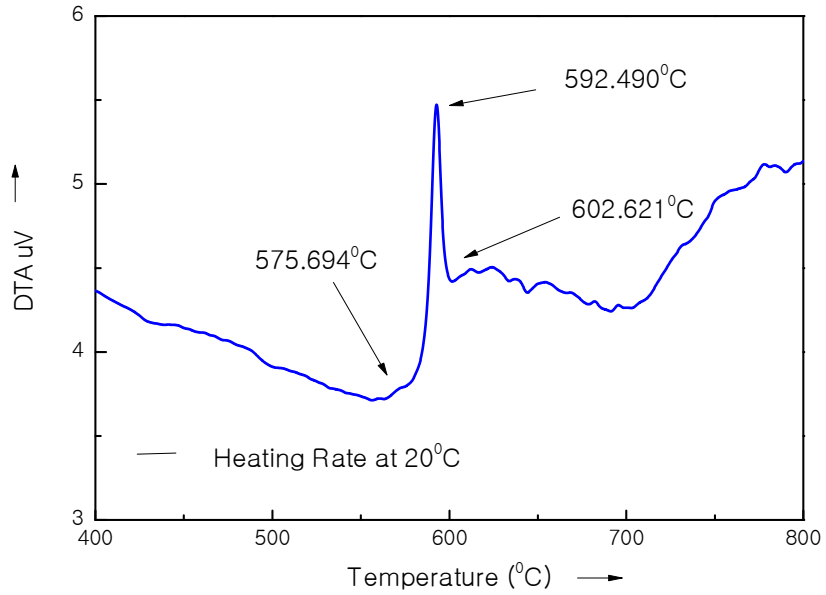

Figure 4.1 (b) : DTA trace of as-cast nanocrystalline amorphous ribbon $Fe_{72.5}Ag_2Nb_3Si_{13.5}B_9$ at the heating rate of 20°C/min

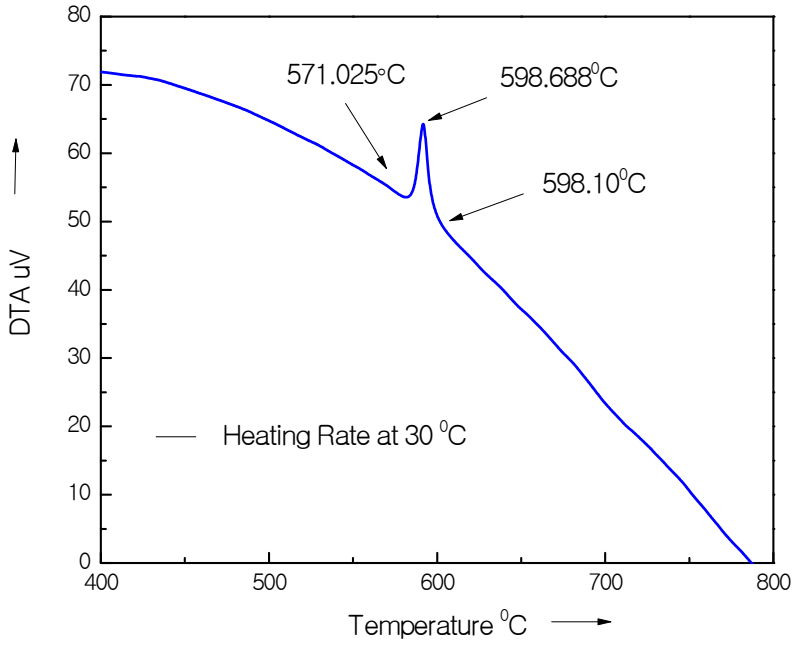

Figure 4.1(c) : DTA trace of as-cast nanocrystalline amorphous ribbon $Fe_{72.5}Ag_2Nb_3Si_{13.5}B_9$ at the heating rate of 30°C/min

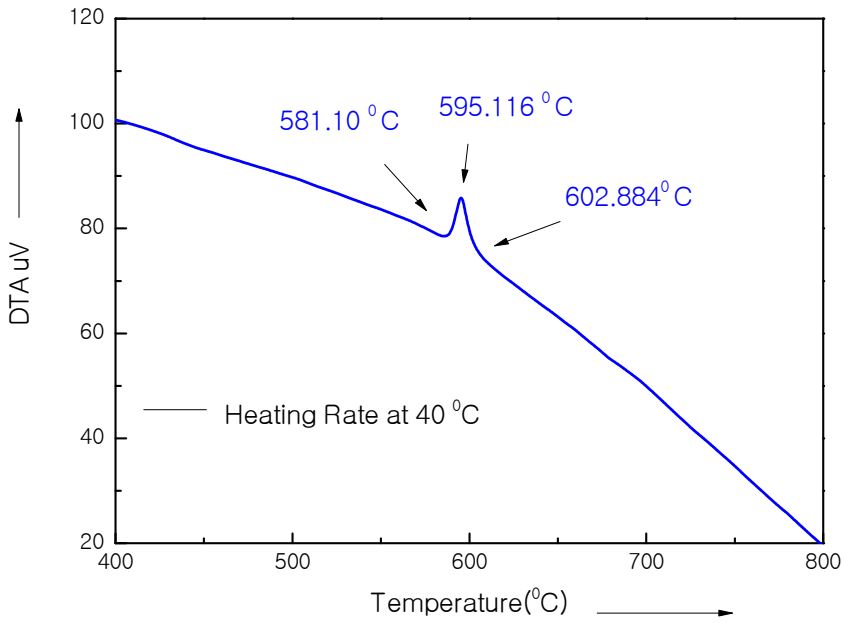

Figure 4.1 (d) : DTA trace of as-cast nanocrystalline amorphous ribbon $Fe_{72.5}Ag_2Nb_3Si_{13.5}B_9$ at the heating rate of 40°C/min

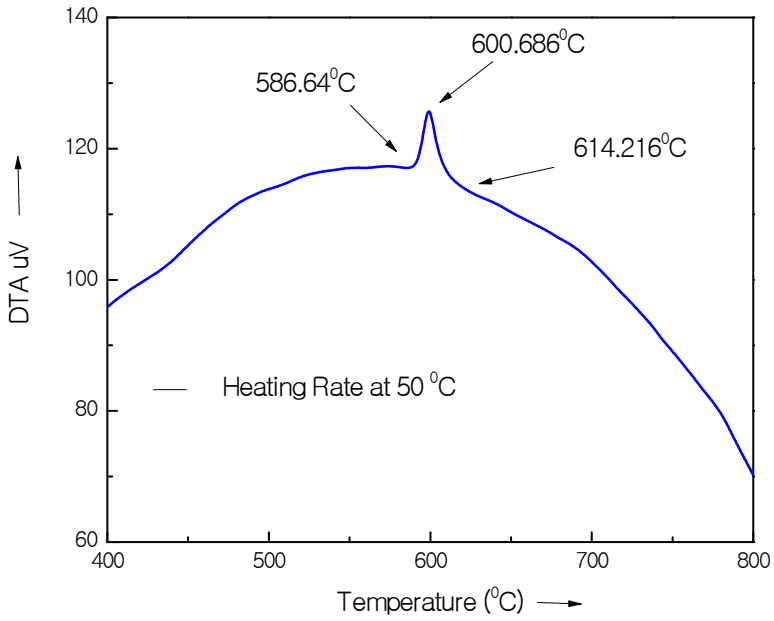

Figure 4.1 (e) : DTA trace of as-cast nanocrystalline amorphous ribbon $Fe_{72.5}Ag_2Nb_3Si_{13.5}B_9$ at the heating rate of 50°C/min

DTA trace of as cast nanocrystalline amorphous ribbon sample recorded in a nitrogen atmosphere with a heating rate 10°C/min has been represented in Figure 4.1 (a). One exothermic peak position is observed at 579°C. The anomaly is followed by

sharp peak, which corresponds to the release of heat of this temperature due to change in the ordering of the atoms.

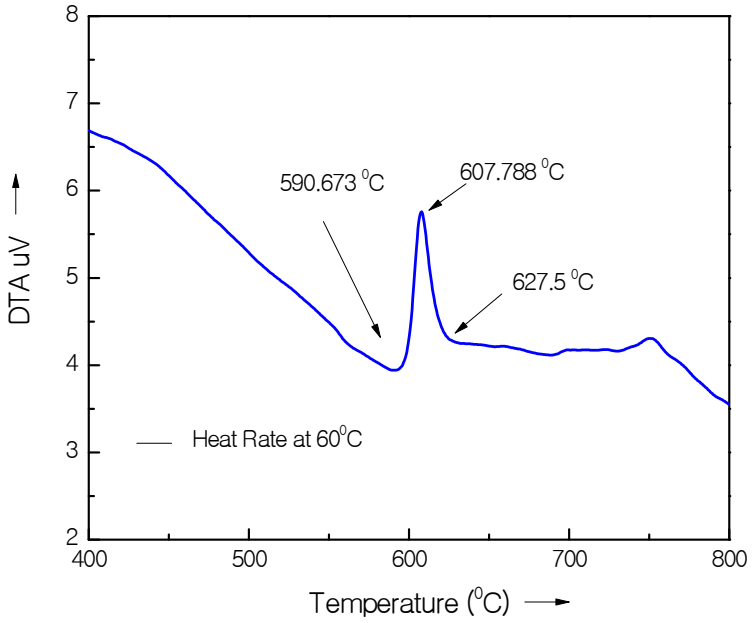

Figure 4.1 (f) : DTA trace of as-cast nanocrystalline amorphous ribbon $Fe_{72.5}Ag_2Nb_3Si_{13.5}B_9$ at the heating rate of 60°C/min

Figure 4.1(a) to Figure 4.1 (f) shows DTA traces and is observed that the 1st. crystallization peak temperature (T_{x_1}) has occurred. That means, it is requires more heat energy for the formation of crystalline phases with increasing heating rates. The crystallization of each phase occurs over a wide range of temperature. It is observed that the crystallization of the phase has occurred over a wide range of temperature and that the peak temperature shift to higher value with the increase of heating rate. The activation energy of T_{x_1}[α-Fe(Si)] has been evaluated using Kissinger plot presented in Figure 4.2(a).

In the case of Ag, the α-Fe(Si) is appeared but due to the lack of providing higher temperature from DTA machine, the Fe_2B phase is not visible. If the DTA of samples would be repeated after crystallization, no peak corresponding to crystallization would be observed. This is quite expected because the specimens were subjected to irreversible transformations. It has been observed that the crystallization temperature range of first phase occurred within 570°C to 630°C. It is also observed

that the peak temperature shift to higher values and crystallization temperature range increase with the heating rates.

Table 4.1: Effect of heating rate on 1st crystallization states of the nanocrystalline amorphous ribbon with composition $Fe_{72.5}Ag_2Nb_3Si_{13.5}B_9$

Heating rate β^0C/min	1st starting $T_{x_1}{}^0$C	1st Peak $T_{p_1}{}^o$C	Temperature range of 1st state in ^{0}C
10	569.69	579	9.31
20	575.69	592.49	16.8
30	571.02	598.68	27.66
40	581.10	595.11	14.01
50	586.64	600.68	14.04
60	590.67	607.78	17.11

This implies that Ag-content alloys weaken the diffusion process to form the crystallization phases since has a melting temperature (961.8^{o}C) lower than that of Fe (1536^{o}C). From our experimental finding it is clearly understood that the partial substitution of Cu and Fe by Ag enhance thermal stability of amorphous alloys against crystallization. For this reason the secondary peak is not found in the range of experimental temperature of DTA.

The activation energy of crystallization of T_{x_1} phase has been calculated using Kissinger equation [4.7].

$$\beta = T_p^2 e^{-E/KT_p}$$

$$\ln\left(\frac{\beta}{T_p^2}\right) = -\frac{E}{KT_p}$$

$$E = -KT_p \ln\left(\frac{\beta}{T_p^2}\right) \qquad (4.1)$$

Where β is the heating rate, T_p is the crystallization temperature, E is the activation energy and K is the Boltzmann constant. The activation energy of T_{x_1}[α-Fe(Si)] phase has been calculated from Table 4.2(a) and using Kissinger's plot shown in Figure 4.2(a) for before annealing. It shows that first thermal crystallization activation energy of α-Fe(Si) phase E_1 is 5.78 eV. The activation energy for formation of the first crystalline $\alpha - Fe(Si)$ phase is slightly than that for the original FINEMET[4.8] composition which is expected due to replacement of Cu by Ag. At this stage,

formation of Ag clusters leads to a small higher activation energy for preferential nucleation. However, with the decrease of crystalline volume fraction, the Ag-rich regions gradually run out. The formation of Ag-rich regions increases the activation energy for nucleation of α-Fe(Si) , so that the α-Fe(Si) phase may nucleate and precipitate preferentially in the Ag-rich regions.

Table 4.2(a) : Effect of heating rate on 1st crystallization of the nanocrystalline amorphous ribbon with composition $Fe_{72.5}Ag_2Nb_3Si_{13.5}B_9$ of calculative data for activation energy calculation data

Heating rate β^0C/min	**Heating rate β^0K/min**	**1st Peak $T_{p_1}{}^oK$**	**1/ T_{p_1} x 10^3**	**ln (β/ $T_{p_1}{}^2$)**
10	13.41	855	1.169	-10.9
20	26.89	865	1.156	-10.23
30	40.24	865.5	1.155	-9.83
40	53.66	868.1	1.152	-9.55
50	67.07	872.5	1.146	-9.33
60	80.46	880.9	1.135	-8.66

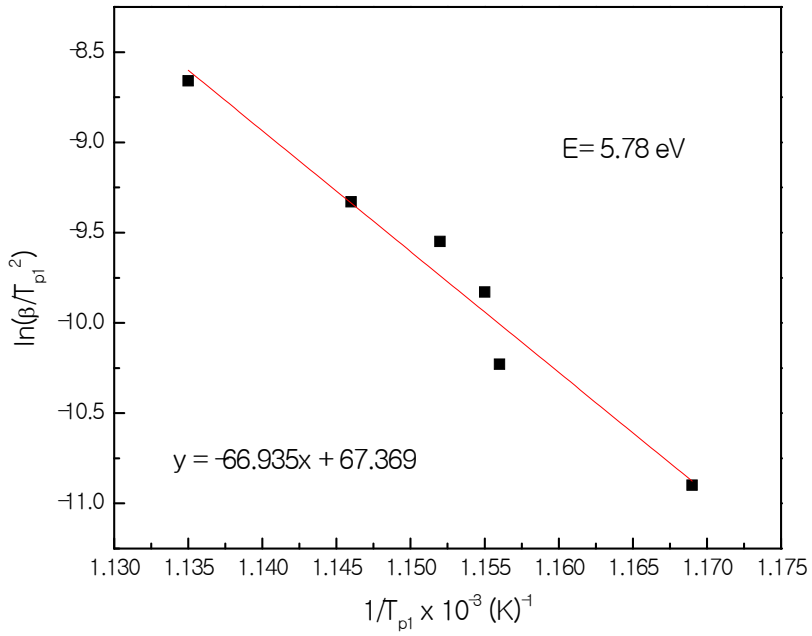

Figure 4.2(a): Kissinger's plot to determine the activation of α-Fe (Si) phase for $Fe_{72.5}Ag_2Nb_3Si_{13.5}B_9$ alloy before annealing

Table 4.2 (b)**:** Comparison of effect of heating rate on 1st and 2nd crystallization states and activation energy of the nanocrystalline amorphous ribbon

Sample	Heating Rate in ^{0}C/min	T_{p1} in ^{0}C	T_{p2} in ^{0}C	E_1 in eV	E_2 in eV
$Fe_{73.5}Cu_1Nb_3Si_{13.5}B_9$[4.16]	10-50	542-570	868-719	3.21	3.81
$Fe_{73.5}Ag_1Nb_3Si_{13.5}B_9$[4.17]	10-50	590-614	767-785	4.37	4.45
$Fe_{72.5}Ag_2Nb_3Si_{13.5}B_9$	10-60	579-608	-----	5.78	-----

4.1.2 Annealing effects on the kinetics of structural relaxation of $Fe_{72.5}Ag_2Nb_3Si_{13.5}B_9$ nanocrystalline amorphous ribbon studied by DTA

The experimental data have been interpreted in terms of different annealing effects on amorphous ribbons of DTA traces at constant heating rate 20°C/min. The DTA traces of $Fe_{72.5}Ag_2Nb_3Si_{13.5}B_9$ alloy in the as cast state and annealed at different temperatures for 2 hrs are shown in Figure 4.3 (a) to 4.3 (d), respectively. Effect of annealing at different temperatures of the amorphous ribbons on their crystallization behavior by DTA scan have been performed on both the samples with continuous heating at 20°C/min heating rate. The effect of annealing on first crystallization peak temperature T_{p_1} corresponds to structural relaxation i.e. release of stress initially formed by rapid solidification.

It is observed from the DTA scan that the onset temperature for the sample $Fe_{72.5}Ag_2Nb_3Si_{13.5}B_9$ annealed at T= 550°C is almost unchanged with respect to its amorphous precursor which is quite logical since T= 550°C is still lower than its T_{x_1} = 579°C.

But the same sample when annealed at T_a = 600^{o}C and 650^{o}C which are higher than the onset of crystallization temperature of T_{x_1} = 579°C, the primary crystallization peak is becoming smaller and display diffused character meaning that substantial amount of primary crystallization, $\alpha - Fe(Si)$ phase has already been completed for 2 hours at T_a= 600°C and T_a = 650^{o}C.

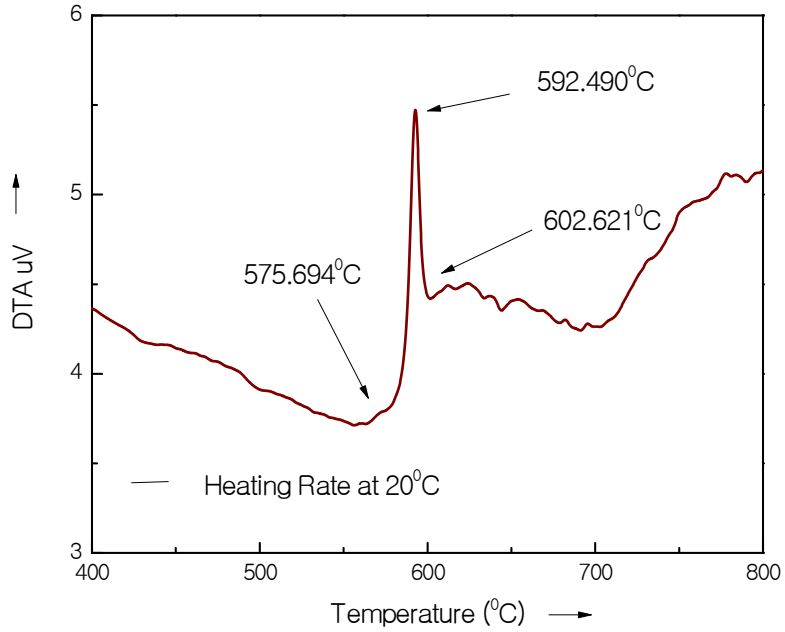

Figure 4.3(a): DTA trace of as-cast nanocrystalline amorphous ribbon $Fe_{72.5}Ag_2Nb_3Si_{13.5}B_9$ at the heating rate of 20°C/min

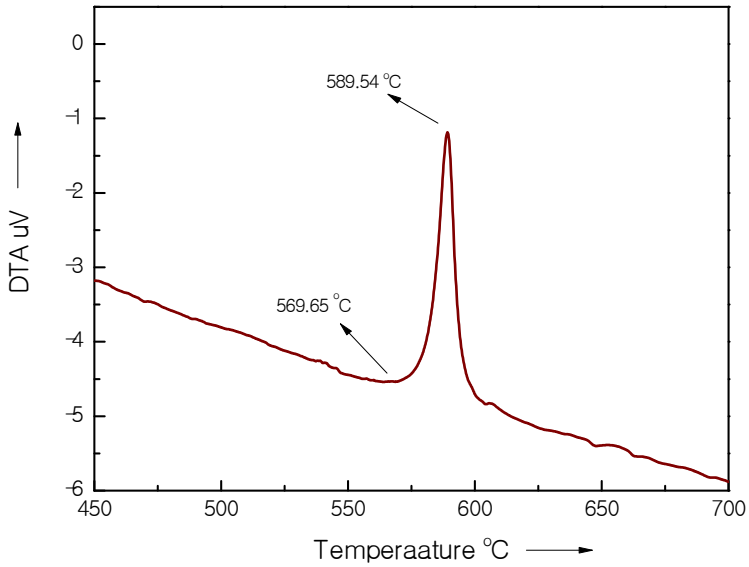

Figure 4.3 (b): Effects on DTA trace of annealing temperature 550°C on the nanocrystalline amorphous ribbon with composition $Fe_{72.5}Ag_2Nb_3Si_{13.5}B_9$ at the heating rate of 20°C/min

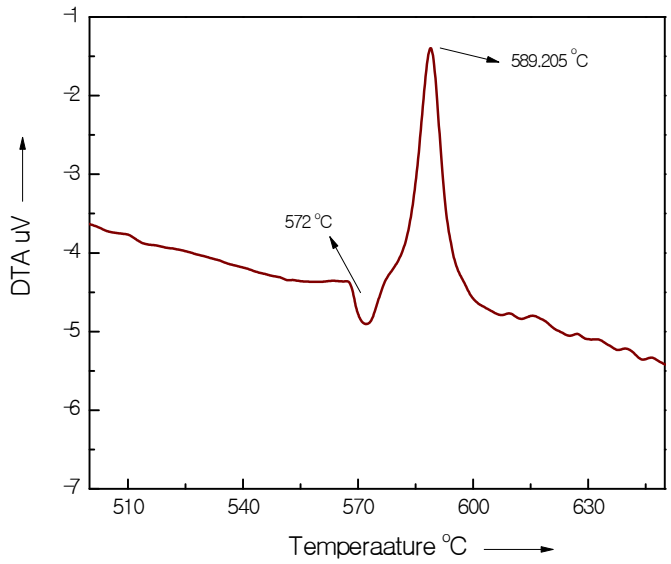

Figure 4.3 (c) Effects on DTA trace of annealing temperature 600°C on the nanocrystalline amorphous ribbon with composition $Fe_{72.5}Ag_2Nb_3Si_{13.5}B_9$at the heating rate of 20°C/min

The area under the first peak of DTA curve corresponds to the crystallization enthalpy, ΔH of $\alpha - Fe(Si)$from which the volume fraction of crystallization (X_f) can be estimated according to the formula,

$$X_f = \frac{\Delta H_a - \Delta H_t}{\Delta H_a} \qquad (4.2)$$

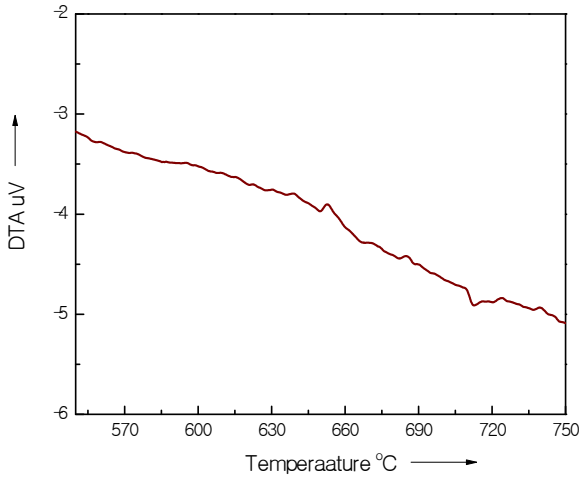

Figure 4.3 (d): Effects on DTA trace of annealing temperature 650°C on the nanocrystalline amorphous ribbon with composition $Fe_{72.5}Ag_2Nb_3Si_{13.5}B_9$ at the heating rate of 20°C/min

where, ΔH_a and ΔH_t are the crystallization enthalpy of the as-cast alloy and that of the alloy annealed for a time t, respectively. This shows that with increasing annealing temperature X_f is expected to increase. The results of DTA scan on annealing of the sample with as-cast sample with the parameter such as T_{x_1} and T_{p_1} are depicted in Table 4.3. As cast and annealed samples at $T_a = 550^oC$ do not show any significant changes area under the peak corresponding to the crystallization enthalpy, ΔH of $\alpha - Fe(Si)$. This means that at $T_a = 550^oC$, no crystallization occurred which is quite obvious since $T_{x_1} = 579^oC$ for this sample. This demonstrates that even annealing at $T_a = 550^oC$, the material still remained amorphous.

Therefore crystallization enthalpy ΔH (area under the peak) is almost equal that of, it's amorphous state. But when annealed at $T_a = 650^oC$, the peak is almost not visible; i.e. $\alpha - Fe(Si)$phase has almost completed.

Table-4.3: Annealing effects on 1st of the nanocrystalline amorphous ribbon with composition $Fe_{72.5}Ag_2Nb_3Si_{13.5}B_9$ at constant heating rate 20°C/min

Annealing Temperature	**Onset Temp. of primary crystallization T_{x_1} °C**	**Primary crys. peak Temperature T_{p_1} °C**
As-cast	575.69	592.49
550°C	569.65	589.54
600°C	572	589.205
650°C	649.36	…….

When the samples are annealed above the T_{p_1}, the primary crystallization as evidenced from their DTA curves are so diffused and smeared that they give signals of nearly completion of the primary crystallization of $\alpha - Fe(Si)$ crystallites. Therefore no characteristic temperatures in this range could be determined.

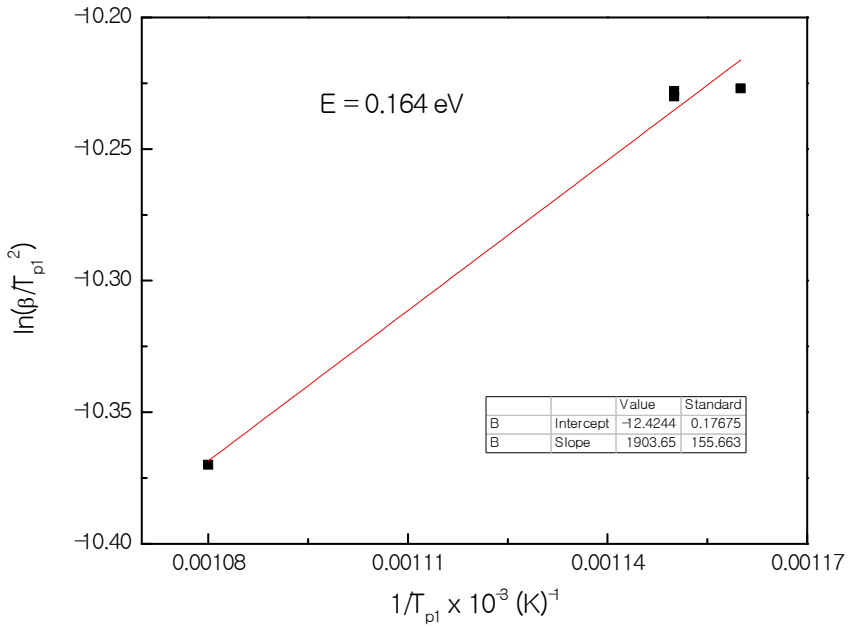

Figure 4.2(b): Kissinger's plot to determine the activation of α-Fe (Si) phase for $Fe_{72.5}Ag_2Nb_3Si_{13.5}B_9$ alloy before annealing

4.2 Microstructural Analysis of Amorphous and Nanocrystalline $Fe_{72.5}Ag_2Nb_3Si_{13.5}B_9$ Alloy by XRD Analysis

XRD experiment has been carried out in order to understand the evolution of microstructure with respect to different annealing temperature 2 hours. XRD has been used to identify crystalline phase in nanocrystalline alloy.In the present work, in order to study the crystallization onset temperature, XRD spectra have been recorded for the nominal composition $Fe_{72.5}Ag_2Nb_3Si_{13.5}B_9$ annealed at 550^{o}C to 750^{o}C for 2 hours. The approximately annealed samples were subjected to XRD by using a MTI Corporation built GSL-1600 x 40 tube furnaces to examine the micro structural evaluation as a function of annealing temperature. From these experiment, obtained results of three kinds of structural parameter including lattice parameter, grain size and silicon content of nanocrystalline α-Fe(Si) grains from which are further attempt to find out the intrinsic and extrinsic magnetic properties. Further attempt to find out the intrinsic and extrinsic magnetic properties as mentioned with evolution of microstructures at different annealing temperatures. There must have some effect of

structural parameters on soft magnetic properties of the alloy which we shall to explain afterwards.

Lattice Parameter of crystalline α-Fe(Si) nanograin was determined at different annealing temperature of the experimental alloys. Structure of the α-Fe(Si) grains depends on the annealing temperature. Generally for an accurate determination of the lattice parameter a number of fundamental peaks are required but in this type of tailored materials upon crystallization only major fundamental peaks (110) is used in calculation of a_o. We have, therefore, determined the lattice parameter using only that particular reflection using equation:

$$2d\sin\theta = n\lambda \text{ and } a_o = d\sqrt{2} \qquad (4.3)$$

Where λ = 1.54053 Å is the wavelength of Cu-K_α radiation and a_o is determined lattice parameter of the grain, d is the inter-planar spacing and θ is the diffraction angle. While grain sizes have been calculated using equation (3.3). One of the most important aims of this study was to determine crystalline grain size for all the annealing temperatures. Grain size of all annealed samples of the alloy composition was determined using Scherrer method [4.9].

Silicon content of the α-Fe(Si) nanograins was calculated from the established quantitative relationship between lattice parameter and Si-content in Fe-Si alloys by Bozorth [4.10]. All the results of θ, d values, full width at half maximum (FWHM) of the intensity peak corresponding to (110) planes, Grain size (D_g) and Si-content from XRD analysis are listed in Table-4.4

It is easy to calculate the Si content in the nanograin from the Pearson hand book relationship [4.11]. From this relationship we have considered a simple equation to calculate Si-content from lattice parameter. This equation is

$$b = -467a_o + 1342.8 \qquad (4.4)$$

where b is at. % Si in the nanograins, a_o is the lattice parameter of nanograins.

4.2.1 Identification of Phases by XRD Experiment

The XRD patterns for the alloy $Fe_{72.5}Ag_2Nb_3Si_{13.5}B_9$ annealed at temperature 550°C, 600°C, 650°C, 700°C, 750°C each for 2 hrs presented in Figure 4.4. In the case of as cast state, there has a broadened peak which could be the evidence of noncrystalline amorphous. It is evident from Figure 4.4 when the sample annealed at 550°C, it exhibited small peak around $2\theta = 45^o$ at the position of d_{110} reflection which

is generally known as diffuse hallow. This diffuse hallow indicates the amorphous nature of the sample. It means at this temperature, no crystallization peak has been detected. So the onset crystallization temperature determined from these results is 550°C. The value of FWHM of the peak at the annealing temperature 550°C was not detected due to the lack of sharp peak. For the higher annealing temperatures, the FWHM value is getting smaller. It shows that the crystallization occurs to a good extent at the higher annealing temperature. The crystallization onset temperatures from DTA experiment for different heating rates were found in the range of 579°C, which shows a good consistency with the XRD results.

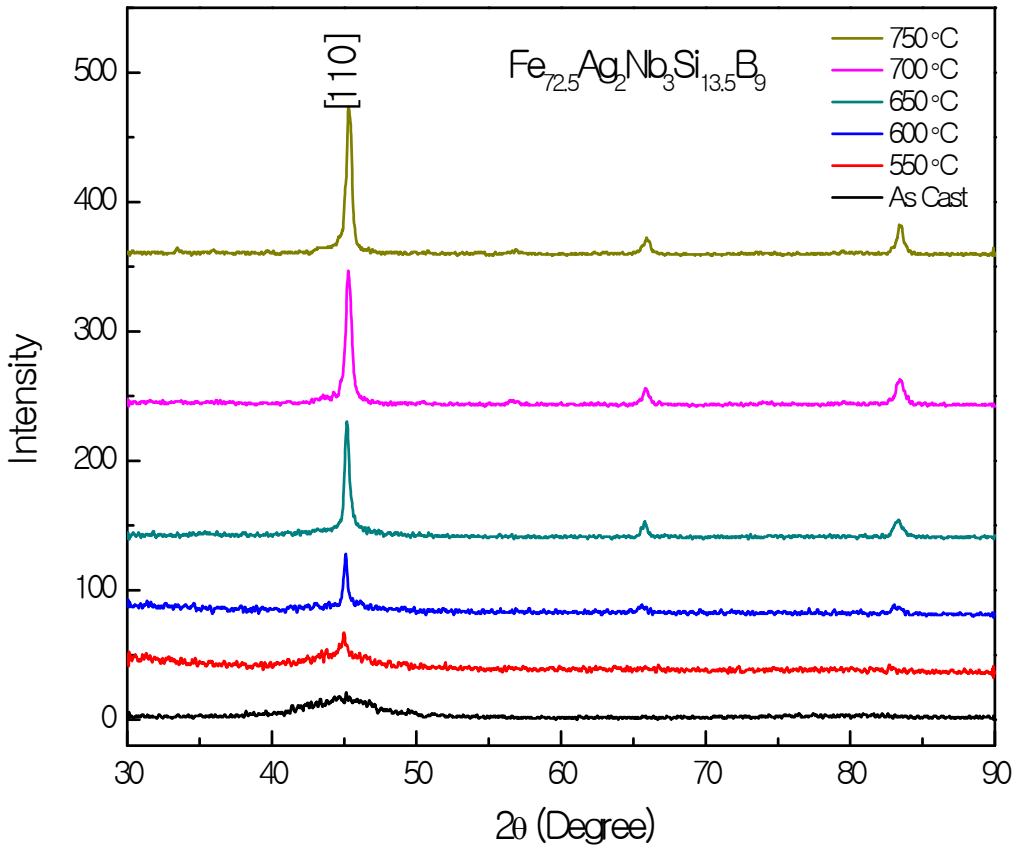

Figure 4.4 XRD spectra of $Fe_{72.5}Ag_2Nb_3Si_{13.5}B_9$ alloys of annealed at different temperatures at constant annealing time 2 hours

For annealing at higher temperature i.e. 600°C, 650°C, 700°C, 750°C the $\alpha - Fe(Si)$ phases were found at the lower values of 2θ at 45.14°, 45.14°, 45.22°, 45.3° respectively with 100% peak intensity on (100) line. Other two fundamental peaks

corresponding to $\alpha - Fe(Si)$ on (200) and (211) diffraction lines for annealing temperature at and above 550^{o}C is obtained in this Figure 4.4. But due to their low intensity they are not clearly visible

From DTA result it is expected that α-Fe(Si) phase would form above 579^{o}C. The XRD pattern illustrated in Figure 4.4 reveal that the difference in Bragg's peak as well as the intensity of the fundamental reflection becomes gradually stronger as the temperature of the heat treatment increases. This increase in the sharpness of the intensity peaks with the annealing temperature indicates that crystalline volume fraction has been increased and also grains become coarser with increased crystallinity. The systematic but negligible shift of peak towards the larger angles with increasing temperature indicates that lattice parameter of the phase gradually decreases due to the increasing of Si-content of α-Fe(Si) phase.

Table 4.4 : Experimental XRD data of nanocrystalline $Fe_{72.5}Ag_2Nb_3Si_{13.5}B_9$ amorphous ribbon at different annealing temperatures

Annealing Temp. in ^{o}C	**θ (deg.)**	**d (Å)**	**B FWHM (deg.)**	**a_0 (Å)**	**D_g (nm)**	**Si (at. %)**
As Cast	22.61	2.0028	…….	1.4161	…..	6.660
550	22.50	2.0121	…….	1.4227	…..	6.629
600	22.57	2.0061	0.3010	1.4185	50	6.648
650	22.57	2.0061	0.2178	1.4185	69	6.648
700	22.61	2.0028	0.2614	1.4162	58	6.659
750	22.65	1.9994	0.2179	1.4137	69	6.670

The lattice parameter, the silicon content in bcc nanograins and grain size of α-Fe(Si) grain can easily be calculated from the fundamental peak of (110) reflections. All results are shown in Table 4.4.

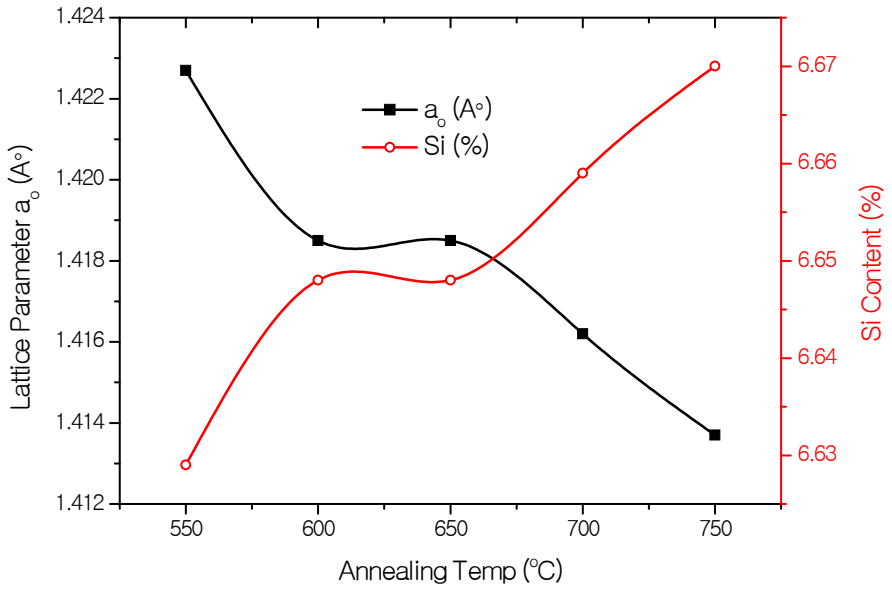

Figure 4.5 Change of Si (at. %) content and Lattice Parameter with different annealing temperature for the sample with composition $Fe_{72.5}Ag_2Nb_3Si_{13.5}B_9$

4.2.2 Lattice Parameter Determination

Lattice parameter of crystalline was determined at different annealing temperatures of the experimental alloys. Structure of the α-Fe(Si) grains depends on the annealing temperature. Figure 4.5 shows that, with the increase in annealing temperature lattice parameter decreasing. The lattice parameter of pure Fe is 2.8664Å. But the lattice parameter at various annealing temperature for the present alloy are significantly less than that of pure Fe. The percentage of partitioned Si in the nanocrystalline α-Fe(Si) phase is maximum at 750^{o}C. After 550^{o}C, increase in Si-content is observed up to 750^{o}C, explained by the fact that at higher temperatures silicon diffuses out of nanograins due to crystallization corresponding to formation of boride phase which is consistent with the result of other FINEMET's. Si having a smaller atomic size compared to Fe, diffuses in the α-Fe(Si) lattice during annealing at different temperatures which results in a contraction of α-Fe(Si) lattice. So the more diffusion of Si, there should be more contraction of the α-Fe(Si) lattice and thereby, the decrease of parameter.

However the decrease in lattice parameter is evident at higher annealing temperature when the diffusion of Si became easier at that temperature due to stress-relief in microstructure caused by heat treatment. Figure 4.5 presents the inverse relationship between lattice parameter and Silicon content. When the sample up to 650^{o}C, the increase of Si-content with subsequent decrease of lattice parameter, as showed in Figure 4.5 indicates that silicon diffuse out of α-Fe(Si) grains for which the size of $\alpha - Fe$ lattice is regained. All the obtained values of lattice parameter in this work are always significantly smaller than that of pure α-Fe. Hence it could be speculated that the metalloid elements of alloy has been dissolved in the b.c.c α-Fe phase.

4.2.3 Silicon Content in Nanograins

Lattice parameter measurements give the hint about a non-negligible solute content establishing the fact that the bcc-ferro-magnetic phase consists of Fe, Ag and Si essentially. The Si contents of the alloy $Fe_{72.5}Ag_2Nb_3Si_{13.5}B_9$ at different annealing temperature 550^{o}C to 750^{o}C for 2 hours are found to be in the range of 6.629% to 6.67%. This small changes with increasing annealing temperature are almost same as Si-content of the amorphous precursor which is about 6.7%. Basically the sequence of recrystallization when silicon diffuses out initiating formation of boride phases but our sample but not seen. All these results are presented in Table 4.4(a) and the pattern of change in Si-content with respect to annealing temperature is represented in Figure 4.5. Figure 4.5 represents the inverse relationship between lattice parameter and Si-content. This kind of relation between lattice parameter and Si-content was observed in the reports [4.12], which are verified in present work effectively. At the initial stage of crystallization lattice parameter first decreases with increase of Si-content, because Si diffuses in the bcc $\alpha - Fe$ phase, to form the soft nanocrystalline $\alpha - Fe$(Si) phase.

4.2.4 Grain Size Determination

In 1963 Kneller et.al.[4.13] studied on nanometric grains. They found that the magnetic properties of isolated grains change drastically as their size is reduced to the nanometer range. When these nanometric grains are consolidated to form a nanostructured material, the magnetic properties are largely determined by the grain size and the exchange interaction between the adjacent grains. Grain size of all

annealed samples of the alloy composition was determined using Sherrer method [4.14]. Grain size was determined using equation (3.3). From Figure 4.4 it is clear that at lower annealing temperature 550^{o}C, the FWHM of the peak is large and with the increase of annealing temperature, the values of FWHM are getting larger. The peaks are, therefore becoming sharper with the shifting of peak position towards higher 2θ value. The peak shifts indicate the change of the values of Si content of the nanograins and therefore, the change of values of lattice parameter of nanograins.

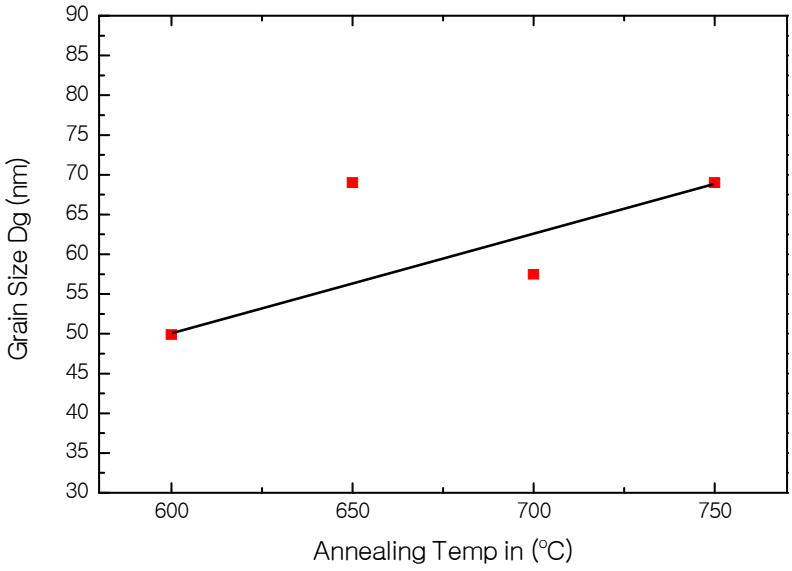

Figure 4.6: Change of Grain Size with different annealing temperature for the sample with composition $Fe_{72.5}Ag_2Nb_3Si_{13.5}B_9$

The increase of annealing temperature initiates partitioning α-Fe(Si) phase and thus grain growth due to formation of nanocrystalline α-Fe(Si) grains. In the range of annealing temperature 550^{o}C to 750^{o}C, the grain size remains in the range of 50 to 69 nm corresponding to soft magnetic α-Fe(Si) phases. In the XRD method much larger area is subjected for investigation. Consequently, problems of statistical significance might arise since a small number of large grains might cause an overestimation of grain size and textured growth which could arise due to ribbon shape amorphous precursor possesses a special problem. The grain size increasing with increasing annealing temperature up to 650^{o}C but further increasing in annealing temperature, the grain size increased which may be resulted due to higher physical distortion and internal strain. These facts reveal that heat treatment temperature

should be limited only 600^{o}C at grain size 50nm to obtain optimum soft magnetic behavior, which will be clear from further experiments in this these.

Table 4.4(b): Comparison of experimental XRD data of grain size at different annealing temperatures of nanocrystalline ribbons

Annealing Temperature in ^{0}C	Grain size of $Fe_{73.5}Cu_1Nb_3Si_{13.5}B_9$ [4.16], D_g (nm)	Grain size of $Fe_{73.5}Ag_1Nb_3Si_{13.5}B_9$ [4.17], D_g (nm)	Grain size of $Fe_{73.5}Ag_2Nb_3Si_{13.5}B_9$, D_g (nm)
550	10	-----	-----
575	11	-----	-----
600	11	-----	50
650	11	10	69
675	14	-----	------
700	22	9	58
750	-----	20	69
800	-----	30	-----

4.3 Magnetic Field Dependence of Magnetization

The magnetization of $Fe_{72.5}Ag_2Nb_3Si_{13.5}B_9$ ribbon is measured as a function of magnetic field using vibrating sample magnetometer (VSM) [4.15]. In this type of magnetometer the sample is vibrated up and down in a region surrounded by several pick up coils. The magnetic sample is thus acting as a time changing magnetic flux; varying inside a particular region of fixed area. The lock-in-action of VSM yields an accuracy of 0.05% of the full scale. The absolute accuracy of this system is better than 2% and the reproducibility is better than 1%.

Least measurable moment is $5x10^{-4}$emu. The magnetometer was calibrated using a high purity-Ni disk. Considering the saturation magnetization of Ni is 54.75 emu/gm at room temperature. The ribbon samples were cut into small shapes, weighed and glued to a standard sample holder.

The magnetization process of the nanocrystalline amorphous ribbon with different field is shown in Figure 4.7. From the magnetization curve it is clearly evidenced that the magnetization is saturated sample in amorphous state within an applied field of 20000 Oe. Saturation magnetization value of M_s =114 emu/gm at

room temperature for original FINEMET is less than the substitution of Fe magnetic moment by the substitution of non-magnetic Ag.

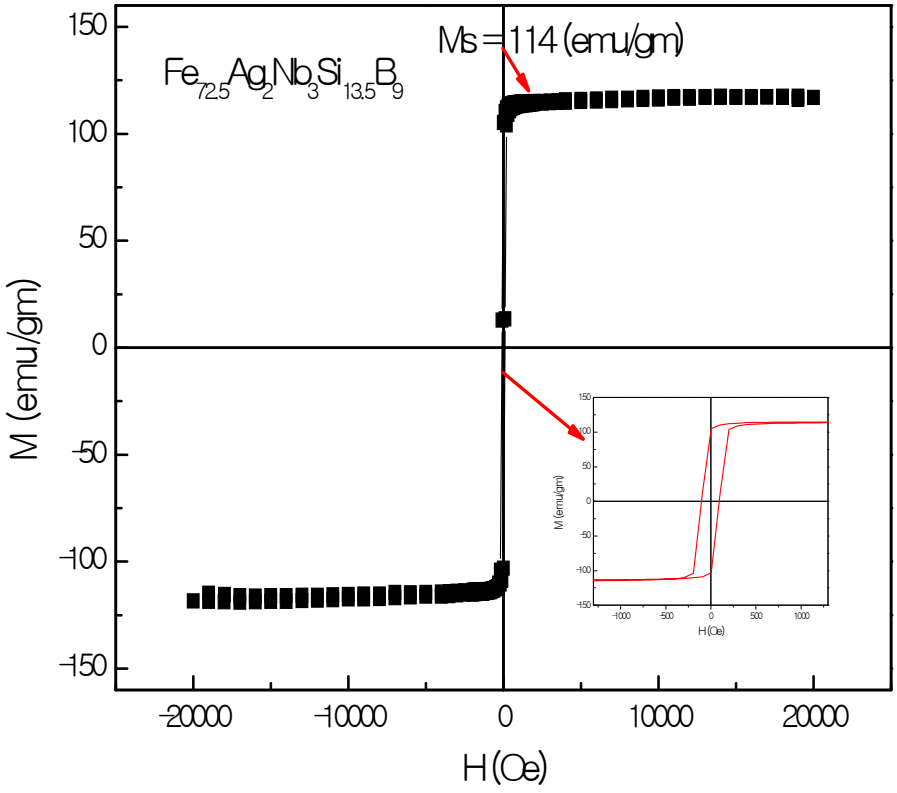

Figure 4.7: Magnetization versus magnetic field curves for the alloy with composition $Fe_{72.5}Ag_2Nb_3Si_{13.5}B_9$

4.3.1 Temperature Dependence of Specific Magnetization $Fe_{72.5}Ag_2Nb_3Si_{13.5}B_9$ Nanocrystalline Amorphous Ribbons

The variation of saturation magnetization (M_s) as a function of temperature in the range 0^oC to 400^oC measured with constant applied field of 10kOe in the amorphous state for the nanocrystalline amorphous samples with composition $Fe_{72.5}Ag_2Nb_3Si_{13.5}B_9$ are shown in Figure 4.8. The magnetization of the sample decreases gradually with increasing temperature since the thermal energy is acting on opposition to the magnetic coupling or exchange energy between neighboring atoms.

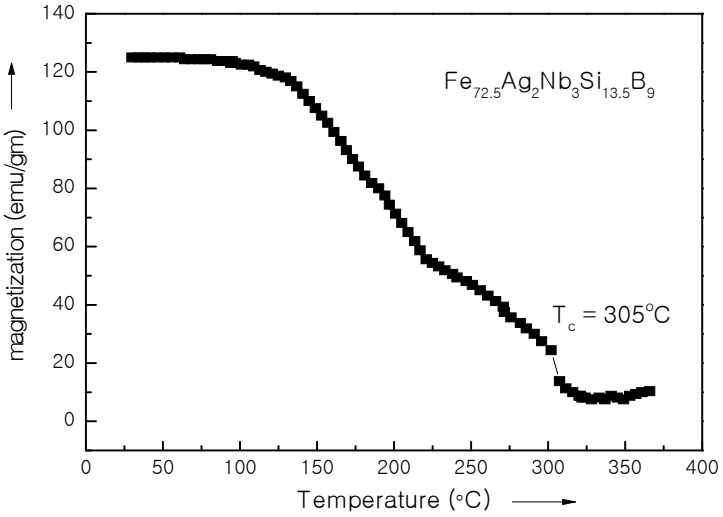

Figure 4.8: Temperature dependence of specific magnetization of amorphous nanocrystalline ribbon with composition $Fe_{72.5}Ag_2Nb_3Si_{13.5}B_9$

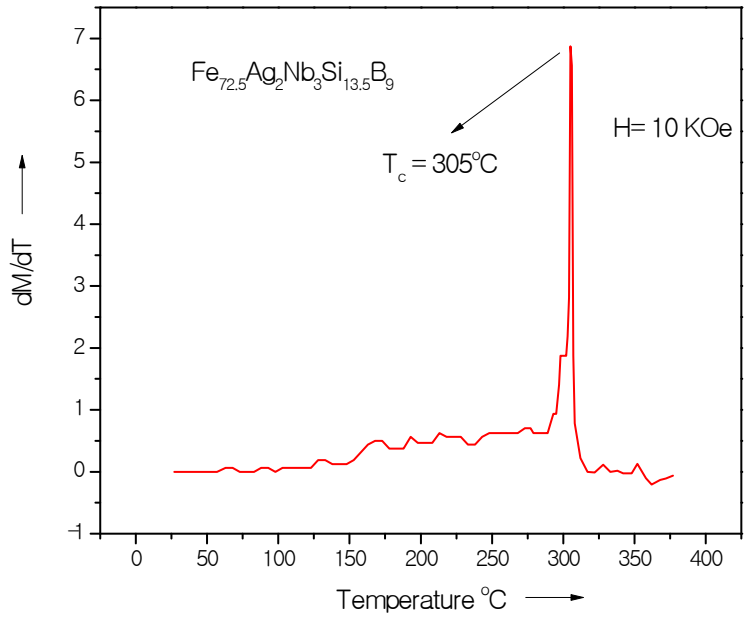

Figure 4.9 : $\frac{dM}{dT}$ versus temperature curve of amorphous Nanocrystalline ribbon with composition $Fe_{72.5}Ag_2Nb_3Si_{13.5}B_9$

It is clearly observed from the curves of Figure 4.8 that the saturation magnetization of the sample decreases gradually. It is also noticed that magnetization

at temperature decreases slowly with the increase of temperature and falls faster the T_c. Therefore during the measurement of T_c of the heating rate should be adjusted in such a way so that no substantial relaxation and crystallization take place. From these curve T_c has been determined as the temperature corresponding to infixion point where the rate of change of magnetization with respect to temperature is maximum shown in Figure 4.8. As the temperature approaches to the T_c magnetization falls more rapidly near to zero as the thermal energy exceeds the magnetic ordering or the exchange energy.

The sharp fall of M_s at T_c indicates that $\frac{dM}{dT}$ versus temperature curve, the material is quite homogeneous for the point to view of amorphousity the sharp fall of M_s are observed at 305^{o}C for experimental sample shown in Figure 4.9. The accurate determination of T_c of amorphous material is really difficult due to irreversible components of the structural relaxation like long range internal stress, topological and chemical short range order. Therefore during the measurement of T_c of the heating rate should be adjusted in such a way so that no substantial relaxation and crystallization takes place.

CONCLUSIONS

5.1 Conclusions

Nanocrystalline amorphous ribbon of FINEMET family with composition $Fe_{72.5}Ag_2Nb_3Si_{13.5}B_9$ were prepared by melt spinning technique and heat treated at various temperatures, below and above the crystallization temperature. This nanocrystalline alloy is as thin as 20-22μm in the amorphous state. This in turn has been aimed at furthering the understanding of crystallization of FINEMET alloys. The crystallization behavior of the sample was investigated by DTA and XRD experiments. The amorphous and annealed samples were examined by XRD to identify the microstructure of the sample. Magnetization measurement as a function of temperature and field were performed by VSM. The magnetic phase transition temperature i.e. Curie Temperature (T_c) was obtained from temperature dependence magnetization measurement. From the systematic investigation on the crystallization structural and magnetic properties the following conclusions can be obtained:

(i) DTA experiments were performed for six different heating rates 10 to 60^{o}C/min. in steps of 10^{o}C/min. up to a temperature of 800^{o}C. DTA reveals, one exothermic peak is distinctly observed which corresponds to crystallization event temperature T_{x_1} [α-Fe(Si)] indicates stability of amorphous state of structural stability and magnetic ordering values of 579^{o}C for $Fe_{72.5}Ag_2Nb_3Si_{13.5}B_9$ with heating rate 20^{o}C/min. The knowledge of crystallization temperature has been fruitfully utilized during the isothermal annealing of this amorphous ribbon for nanocrystallization which ultimately controls the magnetic properties of FINEMET alloy. The saturation temperature is important for stability of α-Fe (Si) phase while it is necessary for fabrication of higher quality inductors.

(ii) The activation energy of the first crystallization phase α-Fe(Si) calculated using Kissinger's plot. Activation energy of α-Fe(Si) phase is 5.78eV. The composition of the alloys affected the crystallization phase because the time needed for the constituent atom to have long range order depends on their bond energies.

(iii) The amorphous stage of the as- cast ribbon has been confirmed by XRD. The evolution of the primary phase on annealed samples has been confirmed as α-Fe(Si) and their sizes

have been determined from the line broadening of fundamental peaks (110) from XRD pattern as affected by annealing around the crystallization temperature. The crystallization phases of amorphous $Fe_{72.5}Ag_2Nb_3Si_{13.5}B_9$ alloy annealed at temperature in the range of 550^0C to 750^0C for 2 hrs is α-Fe(Si) phases with average grain size 47 to 69 nm. These facts reveal that heat treatment temperature should be limited only 600^oC at grain size 50nm to obtain optimum soft magnetic behavior, From XRD experiment, the crystallization onset temperature for the sample is around 600^oC which coincides well with the value obtained DTA.

(iv) The saturation magnetization (M_s) value of sample at room temperature is 114emu/gm. The T_c of samples has been determined by temperature dependence saturation magnetization. The sharp fall of $\frac{dM}{dT}$ versus temperature curve at T_c indicates that the material is quite homogeneous for the point to view of amorphousity. The sharp fall of M_s is observed at 305^oC. For technological uses of nanocrystalline materials at elevated temperature and for thermomagnetic stability for composition that gives higher values of T_c.

5.2 Scope for Future Work

There is much scope for future research in controlling the magnetic characteristics by changing composition and heat treatment certain important parameter like temperature dependence magnetization, anisotropy magnetostriction and Mössbauer effect can be study in detail for a better understanding of microstructure property relationship of Cu replace Ag -based FINEMET type alloys.

REFERENCES

CHPATER-I

[1.1] Yoshizawa Y., Oguma S. and Yamauchi K.; "New Fe-based soft magnetic alloys composed of ultra fine grain structure"; J. Appl. Phys. 64, 6044 – 6046, 1988.

[1.2] Jing Zhi, Kai-Yuan He, Li-Zbi Cheng and Yu-Jan Fu; "Influence of the elements Si/B on the structure and magnetic properties of Nanocrystalline $(FeCuNb)_{77.5}Si_xB_{22.5-x}$ Alloys", J. Magn. Magn. Mater., 153, 315, 1996.

[1.3] Herzer G; "Nanocrystalline Soft Magnetic Alloys"; in Hand Book of Materials, Vol. 10 ed; K. H. J. Buchow, Elsevier Pub. Co. ., 1997.

[1.4] Herzer G; "Grain structure and Magnetism of Nanocrystalline Ferromagnetic"; IEEE Terns. Magn. , 26, 1397 - 1402., 1990.

[1.5] Hakim M. A. and Hoque S. M.; "Effect of Structural Parameters on Soft Magnetic properties of two phase nanocrystalline alloy of $Fe_{73.5}Cu_1Ta_3Si_{13.5}B_9$"; J. Magn. Magn. Mater., 284, 395 - 402, 2004.

[1.6] Sarout Noor, Sikder S. S., Saha D. K. and Hakim M. A.; "Time and Temperature Dependence of Nanocrystalline and Initial Permeability of Finement alloys"; Nuclear Science and Application; 15, 1, 9 - 13, 2016.

[1.7] Mondal S. P., Kazi Hanium Maria, Sikder S. S., Shamima Chowdhury, Saha D. K. and Hakim M. A.; "Influence of Annealing Conditions in Nanocrystalline and Ultra soft Magnetic properties of $Fe_{73.5}Cu_1Nb_3Si_{13.5}B_9$"; J. Mater, Sci Technol., 28(1), 21 - 26, 2012.

[1.8] Müller M. , Matterm N. and Kuhn U.; " Corelation between magnetic and structural properties of Nanocrystalline soft magnetic alloys"; J. Magn. Mater. , 157/158, 209 - 210, 1996.

[1.9] Hakim M. A.; " Magnetic softening of nanocrystalline FeCuNbSiB alloys on annealing"; J. Bangladesh Electronic Society ; 4 , 40-45, 2004.

[1.10] Rahman I. Z. , Kamruzzaman Md. and Rahman M. A.; "Crystallization behavior in Fe-based metallic glass ribbons " ; the 2nd international conference on structure, processing and properties of materials (SPPM) ; Dhaka, Bangladesh, 607-614, 2004.

[1.11] Sikder S. S. and Asgar M. A.; "The kinetics of atomic and magnetic ordering of atomic and magnetic ordering of the Co-based amorphous ribbons as affected by Iron substitution"; Thermochimica Acta, 326, 119 – 126, 1999.

[1.12] Saha D. K. and Hakim M. A.; " Crystallization Behaviour of $Fe_{73.5}Au_1Nb_3Si_{13.5}B_9$" ; Bang. J. Acad. Sci., 30, No.2, 177 - 187, 2006.

[1.13] Asgar M. A. and Sikder S. S.; " Influence of Glass Forming Materials on Atomic and Magnetic ordering of Fe-based Metallic Glass " ; Indian J. Phys. , 73A(4), 493-502, 1999.

[1.14] Khan Z. H., Sikder S. S. , Asgar M. A. and Bhuiyan A. H.; "Effect of annealing temperature on complex permeability of $Co_{80-x}Fe_xSi_{10}B_{10}$ amorphous ribbons"; Bangladesh Journal of Physics, 3(1), 33 - 46, 2007.

[1.15] Alben R. , Becker J. J. and Chi M. C.; " Random anisotropy in amorphous ferromagnets" ; J. Appl. Phys. 49, 1653, 1978.

[1.16] M. Müller and N. Matern; "The influence of refractory element additions on the magnetic properties and on the crystallization behavior of nanocrystalline soft magnetic Fe-B-Si-Cu alloys"; J. Magn. Magn. Mater. 136, 79,1994.

[1.17] Roy P. K.; M. Phil Thesis, Department of Physics, KUET, Khulna, May 2007.

[1.18] Yoshizawa Y. and Yamauchi K.; "Fe-based soft magnetic alloys composed of ultrafine grain structure"; Materials Transaction. JIM. 31, 4, 307-314, 1990.

[1.19] Noh T. H., Lee M. B., Kim H. J., Kang I. K.; "Relationship between crystallization process and magnetic properties of Fe-(Cu-Nb)-Si-B amorphous alloys", J. Appl. Phys 67, 5568, 1990.

[1.20] Kataoka N., Matsunaga T., Inoue A., Masumoto T.; "Soft magnetic properties of b.c.c Fe-Au-X-Si-B (X=early transition metal) alloys with fine grain structure"; Mater. Trans. JIM. 30, 947-950, 1989.

[1.21] Hono K. Hiraga K., Wang Q., Inoue A. and Sakurai T.; Acta Metall. Mater., 40, 2137, 1992.

[1.22] KÖster U., SchÖnemann U., Blank-Bewersdroff, Brauer S., Sutton M. and Stephenson G. B.; Mat. Sci. Eng. A133, 611, 1991.

[1.23] Suzuki K., Makino K., Kataka A., Inoue A. and Masumoto T.; "Soft magnetic properties of nanocrystalline bcc Fe-Zr-B and Fe-M-B-Cu (M =

transition metal) alloys with high saturation magnetization", J. Appl. Phys., 74, 3316, 1991.

[1.24] Alben R., Becker J. J. and Chi M. C.; "Random anisotropy in amorphous ferromagnets", J. Appl. Phys., 49, 1653, 1978.

[1.25] Sawa T. and Takahashi Y., "Magnetic properties of FeCu (3d transition metals) SiB alloys with fine grain structure", J. Appl. Phys., 67, 5565, 1990.

[1.26] Herzer G.; "Grain Size dependence of Coercivity and Permeability in nanocrystalline ferromagnets" IEEE Trans. Mag. 26(5), 1397-1402, 1990.

[1.27] Hakim A., Manjura Haque S.; "Effect of structural parameters on soft magnetic properties of two phase nanocrystalline alloy of $Fe_{73.5}Ta_3Cu_1Si_{13.5}B_9$" J. Magn. Magn. Mater, 284, 395-402, 2004.

[1.28] Manjura Haque S., Hakim A.; "Ultra-soft magnetic properties of devitrified $Fe_{75.5}$ $Cu_{0.6}Nb_{2.4}Si_{13}B_{8.5}$" J. Materials Chemistry and Physics, **101** 112-117, 2007.

[1.29] Biswas K., Ram S., Schultz L., Eckert J.; "Crystallization kinetics of amorphous $Fe_{67}Co_{9.5}Nd_3Dy_{0.5}B_{20}$", Journal of Alloys and Compounds 397, 104–109, 2005.

[1.30] Miguel C., Zhukov A., del Val J.J., Gonzalez J.; "Coercivity and induced magnetic anisotropy by stress and/or field annealing in Fe- and Co- based (Finemet-type) amorphous alloys" J. Magn. Magn. Mater., 294, 245 – 251, 2005.

[1.31] Hakim M. A., Manjura Hoque S., Khalilur Rahman M. and Jamal Uddin Ahamed; "Effect of Cu, Nb, and Si on the characterization behavior and magnetic properties of $Fe_{77}Cu_{0.6}Nb_{2.4}Si_{11}B_9$", Journal of Nuclear Science of Applications, 14, 1, 2005.

Chapter II

[2.1] Mc Henry M.A., Willard M.A. and Laughlin D. E.; "Amorphous and nanocrystalline materials for applications as soft magnets"; Prog. Mat. Sci. 44 291- 433, 1999

[2.2] Mizoguchi T.; IBM Research report, RC 6045, 1976

[2.3] Slawska – Waniewska A., Nowicki P., Lachowicz H. K., Gorria P., Barandiara

J. M. and Hernando A.; “Magnetic interactions in Fe-Zr-B-Cu nanocrystalline materials at elevated temperature”, Phys. Rev. B 50(9), 6465 – 6467, 1994.

[2.4] Bean C. P. and Livingston J. D.; “Superparamagnetism”, J. Appl. Phys. 30(4), S120, 1959.

[2.5] Alben R., Budnic J.I. and Gargil G.S.; a_{111}Metalicglasess, “American SOC. for metals”; 304, 1978

[2.6] Hono K. and Sakurai T.; “Atom Probe studies of nanostructured alloys”; Appl. Surf. Sci. 87/88,166, 1995

[2.7] Hono K., Higara K., Wang Q., Inoue A. and Sakurai T.; “The microstructure evolution of a $Fe_{73.5}\,Nb_3\,Cu_1\,Si_{13.5}\,B_9$ nanocrystalline Soft Magnetic material”; Acta. Metall. Mater. 40(9) 2137-2147, 1992

[2.8] Herzer G; “Nanocrystalline Soft Magnetic Alloys”; in Hand Book of Materials, Vol. 10 ed; K. H. J. Buchow, Elsevier Pub. Co. ., 1997.

[2.9] Yoshizawa Y. and Yamachi K.; “Fe-based soft magnetic alloys composed of ultra-fine grains structure”; Mater. Trans. JIM. (a) 31, 307, 1990

[2.10] Herzer G.; In: Proc of Int. Symp. On 3ab Transition-Semi Metal Thin Films. Magnetism and Processing (Japan SOC for the promotion of Science, Committee, Sendia, Japan) 131 130, 1991

[2.11] Warliment H.; Mater. Sci. Eng. 99, 1988

[2.12] Makino A., Inoue A., Masumoto T.; Mat. Trans. JIM 36, 924, 1995

[2.13] Turnbull D.; “Under what conditions can a glass be formed?”; Contemp. Phys. 10, 473-488, 1969

[2.14] Jones H., Rep. Prog. Phys., 36 1425, 1973

[2.15] Turnbull D., physique J. dc, 35 C4-1,1974

[2.16] Takayama S.; “Amorphous structure and their formation and stability”; J. Materials Sci. Vol. 11(1) 164-185, 1976

[2.17] Irvine J. T. S., Amano E., Huanosta A., Valenzuela R., West A. R.; "Solid State should peak at T_c"; Ionic 40/41, 220, 1990

[2.18] Cohen M.H. and Turnbull D.; "Composition Requirements for Glass Formation in Metallic and Ionic Systems"; Nature 189131-132, 1961

[2.19] Gargil G., III; J. Appl. Phys, 41, 2248, 1970

[2.20] Chen H.S;Acta. Mat. 22, 1505, 1974

[2.21] Nagel and S.R. ,Taue J.; "Nearly- free- electron Approach to the theory of Metallic Glass Alloys"; Phys. Rev. Lett., 35, 380, 1975

[2.22] Berkowitz A. E., Walter J. L., Wall K. F.; " Magnetic Properties of amorphous particles produced by Spark Erosion"; Phys. Rev. Lett. 46, 1484, 1981

[2.23] Murray P. and White J.; "Kinetics of the thermal dehydration of clays"; Trans. Brit. Ceram. SOC. 48, 187-206, 1949

[2.24] Murray P. and White J.; "Kinetics of the thermal decomposition of clay 2, Isothermal decomposition of clay materials"; Trans. Brit. Ceram. SOC. 54, 151-187, 1955

[2.25] Murray P. and White J.; "Kinetics of the thermal decomposition of clay 4, Interpretation of the differential thermal analysis of clays", Trans. Brit. Ceram. Soc. 54, 204-237, 1955

[2.26] Sewel E. C.; "The consequences for differential thermal analysis of assuming a reaction to be first order"; Clay Minerals Bul. 2, 233-241, 1955

[2.27] Kissinger H. E.; "Reaction Kinetics in Differential Thermal Analysis"; Anal. Chem. 29(11) 1702-1706, 1957

[2.28] Boswell F. G.; "On the calculation of activation energies using a modified Kissinger method"; J. Therm. Anal. 18(2) 353-358, 1980

[2.29] Cullity B. D.; "Elements of X-Ray diffraction"; Reading, Addison wesley M.A., 1978

[2.30] Kouvel J.S.; “Magnetism and Metallurgy”; eds. A. Berkowitz and E. Kneller Academic press, New York, 2A,P 523,1969

[2.31] Mc Henry M.E., Willard M.A. and Laughlin D. E.; “Amorphous and nanocrystalline materials for application as soft magnets”; Prog. Mat. Sci. 44, 291-433, 1999

[2.32] Yamaguchi K. and Mizaguchi T.; J. Phys. SOC. Japan, 39, 541, 1075

[2.33] Bozorth R.; “Ferromagnetism”, Van Nostr and D., Princeton N. J.76, 1951

[2.34] Handrich K.; “Conditions for the Existence of Amorphous Ferromagnets” Phys. Stat. Sol.(b) 53, K17, 197

Chapter III

[3.1] Turnbull D.; “Under what conditions can a glass be formed?”; Contemp. Phys. 10, 473-488, 1969

[3.2] Duwez P. , Willens R.H. and kelmentW.Jr.; J Appl. phy. 31, 1136, 1960

[3.3] Coey JMD. and Sun H.; Magn. J. Mater. 87 1251, 1991

[3.4] Schnitzke K., Schultz L., Wecker J. and Katter M.; Appl. Phys. Lett., **57** 2853, 1990

[3.5] H. Le Chatelier; Bull SOC. France Mineral, 10, 204, 1987

[3.6] W. B. Pearson; “A Hand book of Lattice spacing and Structures of Metals and Alloys” (Oxford Pergamon), 1958

[3.7] M. A. Mazid and M. A. Chowdhury; “Design and Construction of Foner type Vibrating Sample Magnetometer”; AECD/MMD/1 (Bangladesh). June, 1986

[3.8] Simon Foner; “Versatile and Sensitive Vibrating Sample Magnetometer”; Rev. Sci. Instr. 30, 160, 1959

Chapter IV

[4.1] Mc Henry M. E., Willard M. A. and Laughlin D. E.; "Amorphous and nanocrystalline materials for applications as soft magnets."Prog. Mat. Sci. 44, 29-433, 1999

[4.2] Manjura Hoque S., Hakim M. A., Chau N.; "Ultra soft magnetic properties devitrified $Fe_{75.5}Nb_{2.4}Cu_{0.6}Si_{13}B_{8.5}$ alloy" Mat. Chem. Phys. 101, 112-117, 2007

[4.3] Saha D. K. and Hakim M. A.; Journal of Bangladesh Academy of Sciences; 30, No. 2, 177-187, 2006

[4.4] Clements W.G. and Cantor B.; in Rapidly quenched metal, Section-1, (eds.Graut N.J. and Giessen B.C.) (MIT Press Cambridge, Mass) P-267, 1976

[4.5] Luborsky F.E.; Materials Sci. Engg. - 28, P-139, 1977

[4.6] Chien, C. L. and Hasegawa, R.S.; "MÖssbauer study of glassy alloys $(Fe-Mo)_{80}B^{20}$" J. Appl. Phys. 49(3) (1978) 1721

[4.7] Kneller E. F. and Luborsky F. E.; "Partical size dependence of coercivity and remanence of single domain partical"; J. Appl. Phys. 34, 656,1963

[4.8] Cullity B. D.; "Elements of X-ray Diffraction"; Adison-Wisley Publishing Company Inc., London, England, P. 262, 1959

[4.9] Pearson W. B.; "A Hand book of Lattice spacing and Structures of Metals and Alloys" (Oxford Pergamon), 1958

[4.10] Mazid M. A. and Chowdhury M. A.; "Design and Construction of Forner type Vibrating Sample Magnetometer"; AECD/MMD/1(Bangladesh), June, 1986

[4.11] Lovas A., Kiss L. F., Balong L.; Magn J.. Mat. Magn., 215-216, 463-465, 2000

[4.12] Holzer D., Perez de Albeniz I., Grossinger R., Sassik H.; Magn. Magn. J. Mater., 203, 82-84, 1999

[4.13] Hakim M. A.; Nuclear Science and Application, 13, 36-43, 2004

[4.14] Knobel K., Sinnecker J. P., Sato Turteli R., Rechenberg N. R., Grossinger R.; J. Appl. Phys., 73, 6603-6605, 1993

[4.15] Berkowitz A. E., Walter J. L., Wall K. F.; Phys. Rev. Lett. 46, 1484-1487, 1981

[4.16] Sarout Noor; M. Phil. Thesis, KUET, p.99, March 2005

[4.17] Asaduzzaman A. K. M.; M. Phil. Thesis, KUET, p.86, Deceember 2016